Catalytic Carbon Dioxide Activation and Sequestration: A Tandem Computational and Mechanistic Analysis

By

Charles Killeen

A Thesis submitted to the Faculty of Graduate Studies of the University of Manitoba in partial fulfillment of the requirements of the degree of

MASTER OF SCIENCE

Department of Chemistry
University of Manitoba
Winnipeg

Abstract:

Carbon dioxide (CO_2) is the major waste product of from the burning of wood and petroleum-derived fuels, and a significant contributor to the greenhouse effect in Earth's atmosphere. Experts fear that the ever-increasing concentration of CO_2 in the atmosphere will continue to have adverse effects on our environment, including making global weather patterns more extreme and increasing the acidity of our oceans. While many countries slowly move towards greener and more renewable sources of energy, the increasing industrialization of developing countries continues to drive global demand for fossil fuels and the CO_2 emissions that follow. Consequently, current strategies for reducing global CO_2 levels must not only focus on reducing emissions but also on the active sequestration of existing CO_2 from the atmosphere. In the following work, a study of CO_2 sequestration chemistry using organic molecular scaffolds is presented which focuses both on analysis of the existing literature and experimental studies of important chemical reactions and species. Throughout this thesis, the reader is presented with a guide to the critical analysis and further development of organic CO_2 sequestration chemistry.

Acknowledgements:

I would first like to thank everyone who has helped and encouraged me during the course of my graduate program at the University of Manitoba, including my friends, colleagues, and family. It is only for their continued support that I kept the motivation necessary to complete this work. I would also like to thank the Department of Chemistry and the Faculties of Graduate Studies and Science at the University of Manitoba for providing me with the necessary resources to complete my work. Thank you as well to my committee members Dr. John Sorensen and Dr. Jake Stout for their guidance in this process and continued willingness to help me when I needed. Finally, I would like to thank my supervisor Dr. Rebecca L. Davis for her passion, teaching, and especially patience which made this all possible.

List of Abbreviations:

°C	degrees Celsius
2-PEI	2-phenylethynylindole
Ac	acetyl
atm	atmospheres pressure
ATR-FTIR	attenuated total reflectance Fourier transform infrared spectroscopy
BSSE	basis set superposition error
Bz	benzoyl
cm	Centimetre
DAD	diode array detector
DBU	1,8-diazabicyclo[5.4.0]undec-7-ene
DCE	1,2-dichloroethane
DCM	dichloromethane
DCMP	diethyl cyanomethylphosphonate
diglyme	diethylene glycol monomethyl ether
DMF	dimethylformamide
DMSO	dimethylsulfoxide
ee	enantiomeric excess
eq.	molar equivalents
Et	ethyl
FT-IR	Fourier transform infrared spectroscopy
h	hours
HPLC	high-performance liquid chromatography
iPr	iso-propyl
iPr*	1,3-Bis(2,6-diisopropylphenyl)-1,3-dihydro-2H-imidazol-2-ylidine
IR	infrared
kcal	kilocalories
kPa	kilopascals
LUMO	lowest unoccupied molecular orbital
M	molarity
m.p.	melting point
Me	methyl
MHz	megahertz
min	minutes
mL	millilitres
mmol	millimolar
mol%	mole percent
MPa	megapascals
MTBD	7-methyl-1,5,7-triazabicyclo[4.4.0]dec-5-ene
N.R.	no reaction

nBu	normal butyl
NHC	N-heterocyclic carbene
nm	nanometre
NMR	nuclear magnetic resonance
P	pressure
PCM	polarized continuum model
Ph	phenyl
psi	pounds per square inch pressure
RDS	rate-determining step
RT	room temperature
SFC	supercritical fluid chromatography
SM	starting material
T	temperature
t	time
TBAI	tetrabutylammonium iodide
TBD	1,5,7-triazabicyclo[4.4.0]dec-5-ene
THF	tetrahydrofuran
THPE	tetrahydropyrimidine-2-ylidine
TLC	thin-layer chromatography
TMG	1,1,3,3-tetramethylguanidine
TON	turnover number
UHPLC	ultra-high-performance liquid chromatography
UV-Vis	ultraviolet-visible light

Table of Contents:

1. Introduction to CO_2 Sequestration Reactions:

There are many different chemical reactions through which carbon dioxide (CO_2) may be transformed into different products, both of academic and industrial importance. Being a cheap and freely available feedstock, capturing and incorporating CO_2 into different molecular structures has the potential to be a high value-added process. In addition, the continued development of CO_2 sequestration reactions may eventually serve to sway the current public opinion of chemical industry as "dirty". The following sections of this chapter provide the reader a brief review that covers the field of organic CO_2 sequestration chemistry from both its industrial roots to its current academic state. This in turn will provide context for the work of the subsequent chapters and convince the reader of the importance and impact of this field.

1.1 Industrially Important CO_2 Sequestration Reactions:

Carbon dioxide sequestering reactions have been of industrial relevance for 160 years, with the discovery of the synthesis of salicylic acid from sodium phenoxide by Kolbe[1] in 1860 marking the first example of such a process. This reaction, which proceeds at 100 atm and 125 °C, is referred to as the Kolbe-Schmidt reaction or Kolbe process and is shown in Figure 1.1. This process is the first half of the industrial route to acetylsalicylic acid and is still performed on a large scale today.

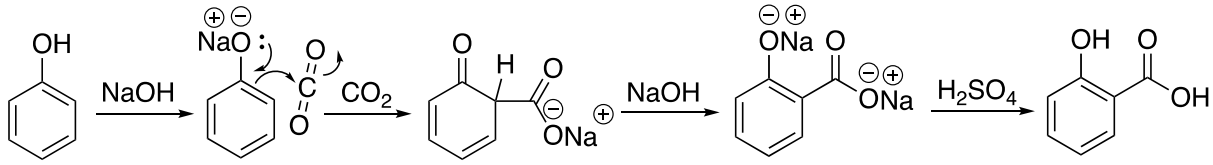

Figure 1.1. Simplified reaction scheme of the Kolbe-Schmidt process.

The largest industrial consumer of carbon dioxide is the Bosch-Meiser process, which produces urea by combining CO_2 with ammonia under elevated temperature and pressure (Figure 1.2).

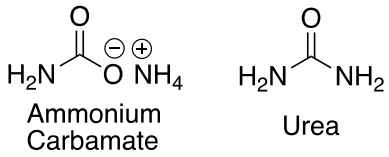

(1) $2NH_3 + CO_2 \rightleftharpoons NH_4^+ \, COONH_2^- \quad \Delta H_f = -117 \, kJ/mol$

(2) $NH_4^+ \, COONH_2^- \rightleftharpoons (NH_2)_2CO + H_2O \quad \Delta H_f = +15 \, kJ/mol$

(3) $2NH_3 + CO_2 \rightleftharpoons (NH_2)_2CO + H_2O \quad \Delta H_f = -102 \, kJ/mol$

Figure 1.2. Chemical structures of urea and ammonium carbamate, and the relevant equations showing the enthalpy of formation of these species individually (1 and 2) and overall (3).

In this process, gaseous CO_2 and liquid ammonia are combined at 110 atm and 160 °C, and an exothermic reaction producing ammonium carbamate occurs.[2] The heat released in this step aids in facilitating the next step, which is the decomposition of ammonium carbamate forming urea and water. Overall, the reaction is quite exothermic, and the heat produced is recovered for use in other areas of chemical plants in which urea is produced. In 2017, 209 megatonnes of urea were produced using this process, which accounts for the conversion of about 97 megatonnes of carbon dioxide to urea and water. This amount of carbon dioxide is equivalent to about 0.27% of yearly anthropogenic CO_2 emissions, or roughly equivalent to the total yearly anthropogenic CO_2 output of Belgium.[2] Interestingly, because ammonia produced from the Haber-Bosch process is made on a such a massive scale as to dwarf urea production, and the production of ammonia often generates carbon dioxide anyway because of the usual necessity of burning fossil fuels to heat reactors, facilities which produce ammonia often install Bosch-Meiser process plants on site to recycle the carbon dioxide they produce.

Carbon dioxide also finds industrial use in the manufacture of various carbonate esters, primarily ethylene and propylene carbonate. These compounds were traditionally made from their respective alcohols(glycols) and phosgene, however new catalytic methods now enable the synthesis of propylene and ethylene carbonate from their respective oxiranes: ethylene oxide and propylene oxide. These reactions take place under pressure and can be facilitated by various catalysts, such as alkali metal iodides, ammonium and phosphonium salts, or Lewis acids. Carbonate esters are valuable specialty solvents, finding use in the polymer, pharmaceutical, and cosmetics industries as semi-volatile highly polar aprotic solvents.[3] The toxicity of carbonate esters is similar to their respective alcohol constituents, which makes propylene carbonate the least toxic option of the commonly employed carbonate esters.

While the previous three products represent the bulk of direct CO_2 usage in industry, these reactions are not considered to be mild processes, due to the high temperatures and pressures they require. Further, other than the Kolbe-Schmidt process which uses two stoichiometric equivalents of base, these reactions form C-O and C-N bonds to the carbon atom in CO_2, which are much more thermodynamically reversible process than C-C bond formation. For this reason, current research focuses on how to activate and sequester CO_2 using chemical transformations that are milder, have lower catalyst loadings, produce products which are more valuable, and especially sequestering CO_2 with C-C bond formation.

1.2 Other Stoichiometric CO_2 Sequestration Reactions:

The capture of carbon dioxide in processes that form C-C bonds under harsh conditions is well established. Organometallic reagents containing the group I and II metals as shown in Figure 1.3 have been known to be capable of forming metal carboxylate salts for over 100 years.[5]

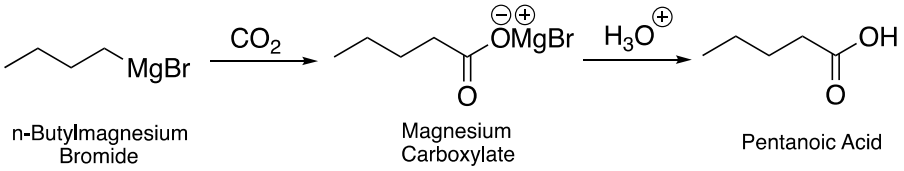

Figure 1.3. Formation of carboxylic acids from Grignard reagents.

This reaction can proceed at ambient pressure and at temperatures well below 0 °C but is only infrequently used as a synthetic strategy due to its very poor functional group tolerance, poor atom economy, and the high reactivity of the starting material. Indeed, CO_2 is generally viewed as something to be rigorously excluded from any reactions containing metals which are relatively electropositive and have low ionic radii, such as those of the s-block and the early transition metals.

More recently, organic base-mediated carboxylation reactions affording C-C bond formation have been reported. In 2008, Jessop et al.[6] reported the α-carboxylation of ketones with 60 bar CO_2 and DBU under solvent-free conditions affording β-keto carboxylic acids, which were subsequently hydrogenated to β-hydroxy carboxylic acids (Figure 1.4).

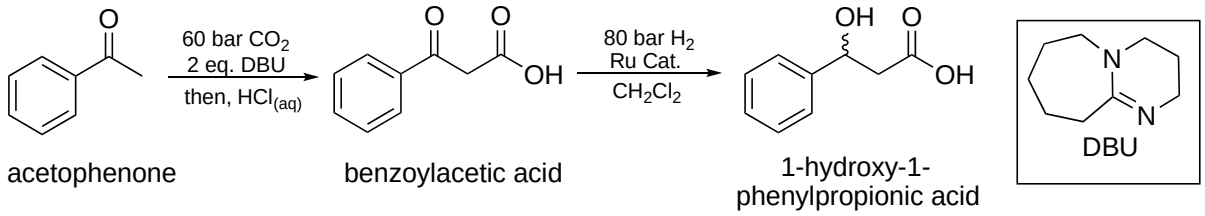

Figure 1.4. Synthesis of β-hydroxy carboxylic acids from Jessop et al.[6]

While this is an elegant CO_2 sequestration reaction, this reaction suffers from a number of caveats which prevent it from being widely applicable. First, while pressures of 60 bar are commonly used in industrial processes, this is beyond the scope of mild laboratory conditions and requires specialized apparatus to be performed safely. Second, the compounds created in the initial carboxylation reaction are unstable. The β-hydroxy carboxylic acids resulting from catalytic hydrogenation are stable, but an extra step is required to actually sequester the CO_2 irreversibly.

Finally, and most pressingly, DBU is very expensive compared to traditional industrial bases such as alkali hydroxides and carbonates. The authors make no note of any attempt to recycle and reuse the DBU, but to do so would require another stoichiometric equivalent of another base to free it from its hydrochloride salt. This is a good example of a C-C bond forming process but suffers from the use of two molar equivalents of DBU and could never be applied to CO_2 sequestration on a large scale, unless it afforded a very valuable product.

1.3 Catalytic CO_2 sequestration reactions:

As in many other areas of synthetic chemistry, recent advances in the field of CO_2 sequestration have focused on developing chemical transformations which proceed through catalytic processes. Of specific interest are the processes which achieve these transformations using metal-free catalysis, however metal-free processes are not yet widely applied to C-C bond forming sequestration reactions. In the following section, a two-part review of the current state of the field is presented. The first part consists of a focus on specific mechanistic insights derived from metal-free carbon-heteroatom bond forming reactions, while the second part focuses on reactions which form C-C bonds with CO_2. These latter reactions are the most difficult to achieve and of greatest academic interest, and thus metal catalyzed processes are presented as they have increased relevance in this context. To date, only one example of an organocatalytic C-C bond forming CO_2 sequestration reaction has been reported.

1.3.1 Carbon-Heteroatom Bond Formation:

One such example of a C-O bond forming CO_2 sequestration reaction which exemplifies the principles of green chemistry and catalysis is the following work by Fan *et al*. shown in Figure 1.5.[7] Herein the authors reported the transformation of CO_2 and aryl epoxides into cyclic carbonate esters catalyzed by charge-containing thioureas and promoted by tetrabutylammonium iodide

(TBAI). The reaction proceeds in high yield under very mild conditions, with low loading of catalyst and promoter, and without the use of solvent.

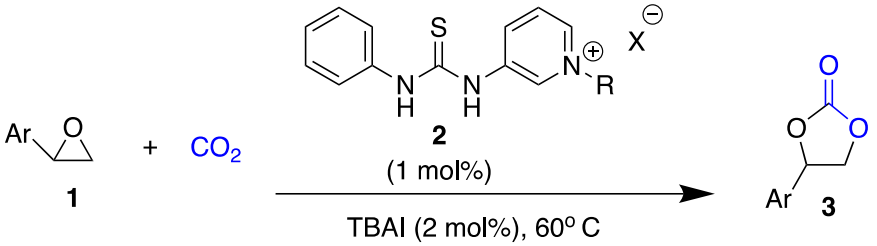

Figure 1.5. Synthesis of cyclic carbonate esters catalyzed by charge-containing thioureas and TBAI.

Using a test substrate of 2-phenyloxirane **1**, the thiourea catalyst **2** with R= methyl and X= iodide was found to be best at promoting the transformation. Detailed in Figure 1.6, the authors propose a catalytic cycle that beings either with direct attack on the less hindered carbon of the epoxide by the sulfur atom of the thiourea, or by initial ring-opening with iodide followed by displacement by the sulfur of the thiourea. This process activates the epoxide oxygen atom as a nucleophile which then attacks the central carbon of CO_2, forming a negatively charged carbonate hemiester. This species in turn attacks the carbon atom which is bonded to the catalyst, turning over the catalyst and generating the carbonate ester product **3**.

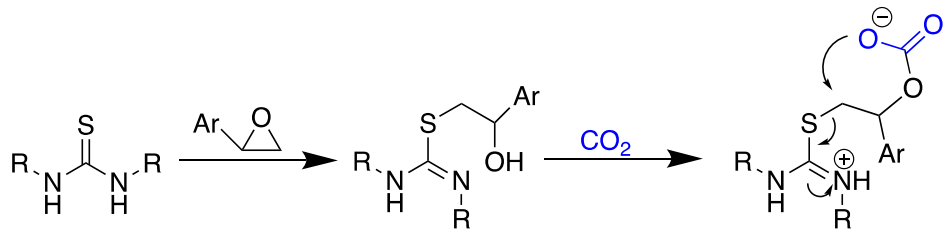

Figure 1.6. Simplified catalytic cycle of Fan *et al.* showing epoxide activation by the thiourea catalyst.

To further probe their proposed mechanism, the authors performed a series of calculations to determine the specific role of the TBAI additive in the transformation. They found that the intermediate resulting from the nucleophilic attack of the thiourea sulfur atom on the substrate was 13.3 kcal/mol more stable than the intermediate resulting from nucleophilic attack by iodide.

However, the direct barrier to this intermediate of 46.8 kcal/mol was reduced to 25.5 kcal/mol when proceeding through the intermediate formed through initial attack by iodide on the substrate. As tertiary ammonium iodides are common additives in organocatalytic CO_2 sequestration reactions, this finding is an important insight into their specific role in these reactions. In essence, the iodide ion acts as a kinetic nucleophile, reducing the barrier to the thermodynamic product containing the thiourea catalyst, which follows given the greater steric bulk of the thiourea catalysts compared to iodide.

In addition, when enantiopure (R)-**1** was subjected to the reaction conditions, the (R)-carbonate ester product **3** was obtained in 86% ee. This was increased to >99% ee when the substrate was changed to 2-(benzyloxymethyl)oxirane, which eliminates the potential for *in-situ* racemization caused by the positive charge buildup on the benzylic position of the initial substrate. This finding demonstrates the potential ability of this transformation to be applied in the derivatization of the existing chiral pool and also demonstrates well the mild conditions of the reaction. This work is also important as a demonstration of an all-sp^3 hybridized CO_2 sequestration reaction, which are currently rare.

Another particularly interesting C-O bond forming CO_2 sequestration reaction was reported by Zhou *et al.* and involves the synthesis of carbonate esters from substituted propargylic alcohols (**4**) using a CO_2 derived catalyst.[8] In this process shown in Figure 1.7, propargyl alcohols and CO_2 combine under solvent-free conditions at 60 °C and 2.0 MPa with 5 mol% catalyst to form cyclic carbonates (**5**) in moderate to high yields.

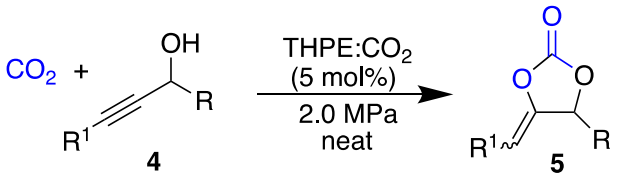

Figure 1.7. Synthesis of cyclic carbonate esters from CO_2 and propargylic alcohols catalyzed by THPE:CO_2.

The catalysts used are derivatives of alkylamidinium halides(**6**), which have been deprotonated and carboxylated with CO_2 to form zwitterionic tetrahydropyrimidine-2-ylidine (THPE) carboxylates (**8**) as shown in Figure 1.8.

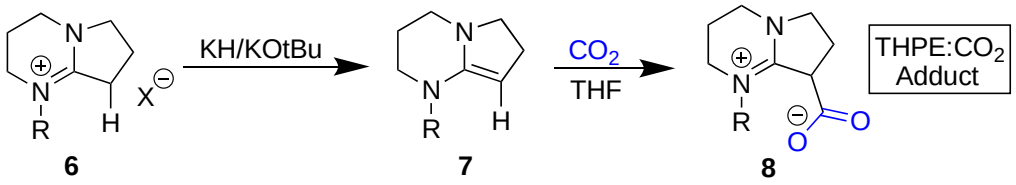

Figure 1.8. Synthesis of THPE:CO_2 adducts from alkylamidinium salts and CO_2.

The intrigue of this reaction arises from the fact that species similar to **8** are often invoked as on-cycle intermediates in catalytic cycles, being proposed to represent an "activated" form of CO_2.[9,10,11] However, in this work the authors propose that this THPE:CO_2 adduct is actually an active catalyst through a series of mechanistic studies. First, although the neat reaction of CO_2 and **4** with 5 mol% **8** proceeds to >90% yield in two hours, no formation of **5** is observed in that time when heating the substrate and catalyst in the absence of CO_2. In addition, conducting the reaction under standard conditions using ^{13}C-**8** did not result in the production of an isotopically enriched product, and conducting the reaction under an atmosphere of $^{13}CO_2$ led to an isotopically pure product containing the cyclized $^{13}CO_2$. **8** was also subjected to thermodynamic stability studies and showed no decomposition to free CO_2 and **7** in 2h at 100 °C in DMSO. Based on this, the authors propose a mechanism of activation shown in Figure 1.9 where the carboxylate of **8** bonds to the hydrogen atom of **4** and allows for the insertion of CO_2 into the O-H bond to form a

negatively charged carbonate hemiester, which then cyclizes with the alkyne moiety of the substrate. The protonated carboxylate of the catalyst then transfers the proton to the formed carbanion, forming **8** and regenerating the active catalyst.

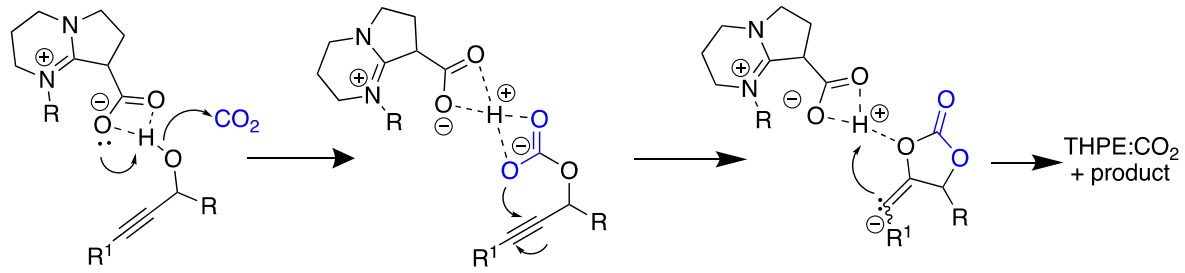

Figure 1.9. Key steps from the catalytic cycle proposed by Zhou *et al.* for the reported reaction.

Although the viability of this reaction proceeding exactly as the authors show in their proposed catalytic cycle is questionable, their mechanistic studies suggest that at least it is likely the carboxylate group of **8** is not fluxional during the reaction conditions they use. If accurate, this result is significant to the field of organocatalytic CO_2 sequestration reactions as zwitterionic CO_2 adducts are typically thought to be on- or off-cycle intermediates, and not active catalysts in these reactions.

Similar to the previous example, the ability of propargylamines (**9**) to incorporate CO_2 into an oxazolidinone scaffold (**10**) detailed in Figure 1.10 has also been shown.[12]

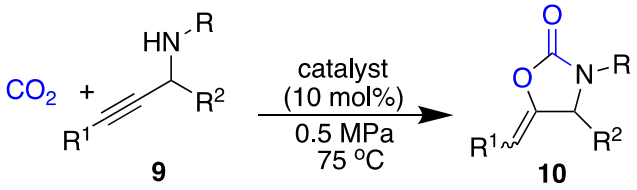

Figure 1.10. Synthesis of oxazolidinones from CO_2 and propargylamines catalyzed by nitrogenous bases.

In this work the authors compare the reactivity of the two guanidine derivatives shown in Figure 1.11, 1,1,3,3-tetramethylguanidine (TMG) and 1-methyl-1,5,7-triazabicyclo[4.4.0]dec-5-ene (MTBD), both of which are capable of catalyzing the transformation.

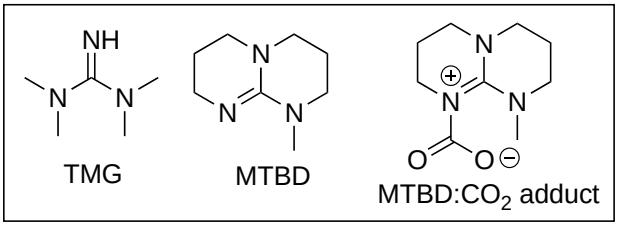

Figure 1.11. The two guanidine derivatives studied and an example structure of a CO_2 adduct.

In-situ ATR-FTIR spectroscopy was used to study the reaction of these compounds with CO_2 in THF. When MTBD was exposed to an atmosphere of CO_2, two new IR peaks appeared, which were ascribed to the C=N (1602 cm^{-1}) and C=O (1648 cm^{-1}) stretches. However, when TMG was subjected to the same conditions, no new peaks in the area were observed, suggesting it is incapable of complexing CO_2 and forming a similar adduct. When the authors added an excess of water to the solution of MTBD:CO_2 in THF, they were able to observe a change in the IR spectrum, and characterize the resulting product as [$MTBDH^+$][HCO_3^-]. The authors then compared the ability of TMG and MTBD to catalyze the CO_2 sequestration reaction with **9** in DMSO and acetonitrile, at different catalyst loadings and with or without water present. They found that at 10 mol% MTBD in acetonitrile the reaction would proceed to completion with or without the presence of a molar excess of water. However, when the catalyst loading was lowered to 1 mol% the reaction would only proceed to <10% completion in the allotted timeframe. When the same reaction was performed with TMG in DMSO, it was similarly able to proceed to completion with or without excess water. Interestingly, when the catalyst loading was lowered to 1 mol% TMG, the reaction proceeded tenfold faster in the presence of water. These findings are quite unique, as most other CO_2 sequestration reactions are thought to necessitate dry conditions. The fact that excess water seems to have no effect on the reactions at 10 mol% loading but has an opposite effect between the two catalysts tested at 1 mol% suggests that the nature of water in these systems is of potential importance. The authors make no assertion of what they think the role water plays in this reaction

is, but do make note that their 1 mol% TMG/water system is substantially better than the 10 mol% MTBD used in the literature upon which the study was based.[13]

In summary, these three examples of carbon-heteroatom CO_2 sequestration reactions are all very important to the field because of the unique findings they present. These works emphasize the importance of understanding the exact nature of the interaction between CO_2 and all components of a reaction. In particular, the demonstration that catalyst:CO_2 complexes can be inert, active, or even absent in these transformations is especially important for further study and development of CO_2 sequestration reactions.

1.3.2 Carbon-Carbon Bond Formation:

Just as CO_2 sequestration reactions which form carbon-heteroatom bonds rely on the initial deprotonation of a heteroatom to activate it as a nucleophile, the reactions which form carbon-carbon bonds rely on the initial formation of a nucleophilic carbanion or carbanion equivalent. Two examples of this concept are the works by the group of Tohru Yamada shown in Figure 1.12, in which enolates serve as the nucleophilic carbon source.[14,15] These works, similar in their use of 4 eq. MTBD and catalytic silver(I), differ only by the relative arrangement of the enolizable positions in the substrate scaffolds **11** and **13**.

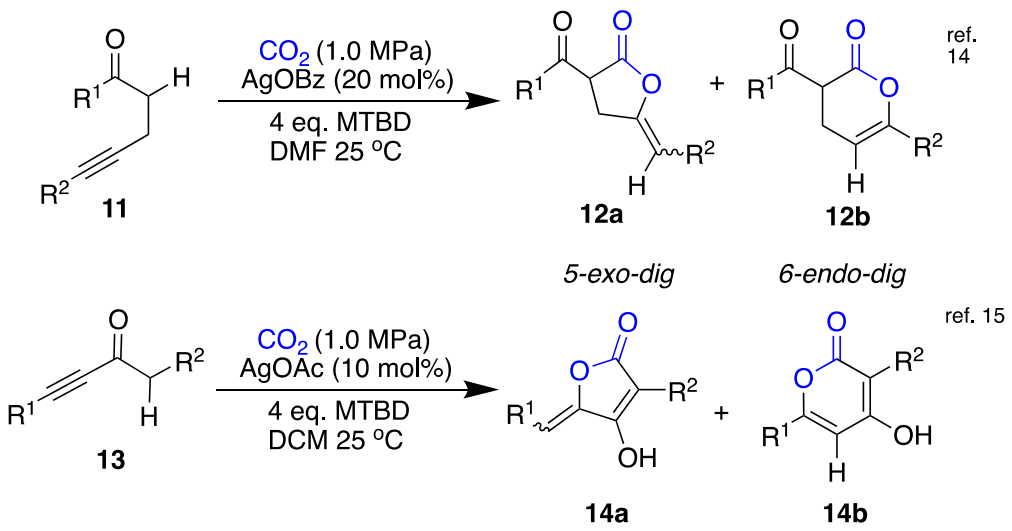

Figure 1.12 Two silver-catalyzed reactions from the Yamada group which use internal[14] and external[15] enolate nucleophiles and alkyne electrophiles to incorporate CO_2 into heterocyclic rings.

In the development of these reactions, the *6-endo-dig* products **12b** and **14b** were both obtained as minor products in most cases, with optimized conditions being very selective (>95:5) for the *5-exo-dig* products **12a** and **14a**. Interestingly, in the first example, the use of Au(III) instead of Ag(I) as the metal catalyst reduced the yield significantly, but lead to the formation of **12b** as the major product. In the second example, **14b** was only formed in small amounts when the R^2 group was very sterically bulky.

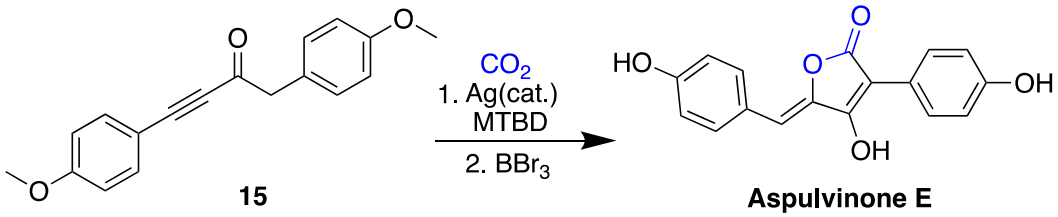

Figure 1.13 Two-step silver-catalyzed synthesis of Aspulvinone E from alkynone and CO_2.

Here, the authors report the synthesis of Aspulvinone E in two steps, starting from the di-(paramethoxyphenyl) substituted alkynone **15** as shown in Figure 1.13. In the first step CO_2 is incorporated into the scaffold following the reported reaction conditions, forming the core tetronic acid heterocyclic scaffold of the molecule. In the second step, the p-methoxy substituents are

demethylated by boron tribromide forming the diphenolic final product, which is a yellow pigmented compound produced by fungi of the genus *Aspergillus*.[16]

In both of these works, Yamada asserts that the role of the transition metal catalyst is as a Lewis acid, activating the alkyne moieties of the substrates as electrophiles. While in the first publication the authors examine a limited scope of metal catalysts, the later one indicates no scope of metal catalyst testing; silver(I) acetate was the only metal catalyst used. This is a troubling assertion because in both works it is simply assumed that the only possible role of the metal is as a Lewis-acidic alkyne activator, and thus only metal catalysts from groups 10 and 11 were tested. While the softer, more electronegative late transition metal ions are well known to readily coordinate alkynes and activate them as electrophiles, this begs the question: why has alkyne activation in this manner proven to be unnecessary in the carbon-heteroatom bond forming CO_2 sequestration reactions? The heteroatom nucleophile examples of section 1.3.1 are all metal free, and in many cases MTBD is used catalytically to facilitate the reactions, while the Yamada reactions with **11** and **13** rely on it in excess. Whether a CO_2 sequestration substrate is initially carboxylated at a carbon atom or a heteroatom, the subsequently formed nucleophile which attacks the alkyne moiety is the same in all cases; the carboxylate anion formed from CO_2. Because of this discrepancy, it is possible that transition metal catalysts play a different role in these C-C bond forming reactions than is currently thought.

To date, there has been only one example of a CO_2 sequestration reaction which proceeds through C-C bond formation that uses catalytic base and is metal-free.[9] This work, reported in 2015, uses an indole nucleophile and the typical alkyne electrophile to afford the tricyclic pyrano[4,3-b]indol-1(5H)-one product shown in Figure 1.14.

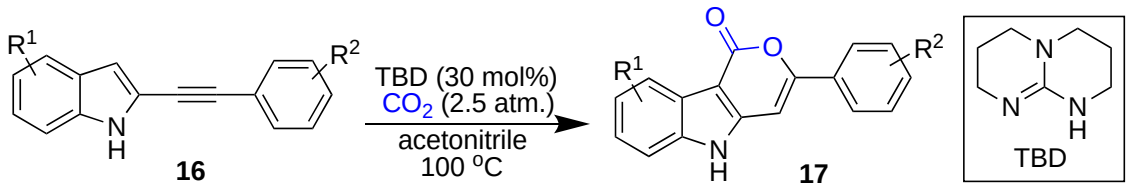

Figure 1.14. Organocatalytic CO_2 sequestration reaction from Skrydstrup *et al.*

This reaction, other than being metal-free, can be considered similar to the work of the Yamada group. Similar to anilines, indoles contain within their scaffold a trapped enamine which makes them ambident nucleophiles, capable of reacting through either the 1- or 3- positions as shown numbered in Figure 1.15.

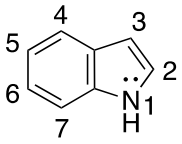

Figure 1.15. Numbered positions of the indole scaffold.

Considering the relationship between enamines and enolate anions, the ability for this scaffold to act as a carbon nucleophile is clearer. In their publication, the authors claim to have been inspired by a reported carboxylation reaction of unprotected indoles with lithium t-butoxide[17], which they reasoned could be conceptually combined with the previously discussed reactions which trap CO_2 with heteroatom nucleophiles and alkyne electrophiles. Initially, the authors attempted to use organic superbases and gold(I) catalysis to achieve this transformation, but subsequently found that the reaction would proceed to completion with only 2 equivalents of DBU. Inspired by this result, a scope of organic superbases was tested, and 30 mol% TBD was found to be capable of facilitating the reaction with **16** to form **17** in 20 hours. The transformation was found to be tolerant of a wide range of substituents on both the indole moiety and the alkyne moiety, with alkyl-, heteroaromatic-, and substituted phenyl- acetylenes all affording products in moderate to high yields. Of all reported substrates, only the unsubstituted C-H terminated alkynylindole suffered

poorer yields. Of the bases tested in catalytic amounts, only DBN, TBD, and MTBD were found to achieve turnover, whereas other commonly employed CO_2 sequestration reaction catalysts such as TMG and the carbene iPr* did not afford any product. Interestingly, in contrast with the work of Yamada, this transformation was specific for the *6-endo-dig* product, and no *5-exo-dig* products were ever observed. The authors performed a few small mechanistic studies, noting that the analogous *6-endo-trig* cyclization reaction with the alkenyl substited **18** as in Figure 1.16 was not viable.

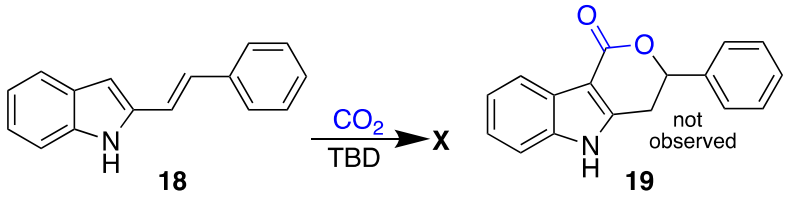

Figure 1.16 The unsuccessful *6-endo-trig* cyclization reaction scheme.

In addition, it was observed that the indole scaffold **20** with a protected nitrogen atom and a carboxaldehyde group on the 3-position shown in Figure 1.17 would immediately form the three-membered cyclic product **21** upon oxidation of the aldehyde to the carboxylate.

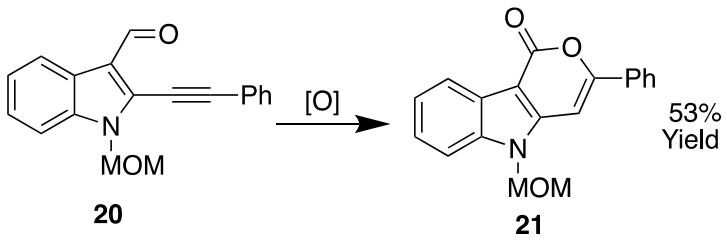

Figure 1.17. Spontaneous cyclization of the substrate upon oxidation of the aldehyde to a carboxyl group.

Finally, the authors proposed the catalytic cycle in Figure 1.18 for this reaction, which they assert progresses via CO_2 being activated as an electrophile through the initial formation of a base:CO_2 adduct.

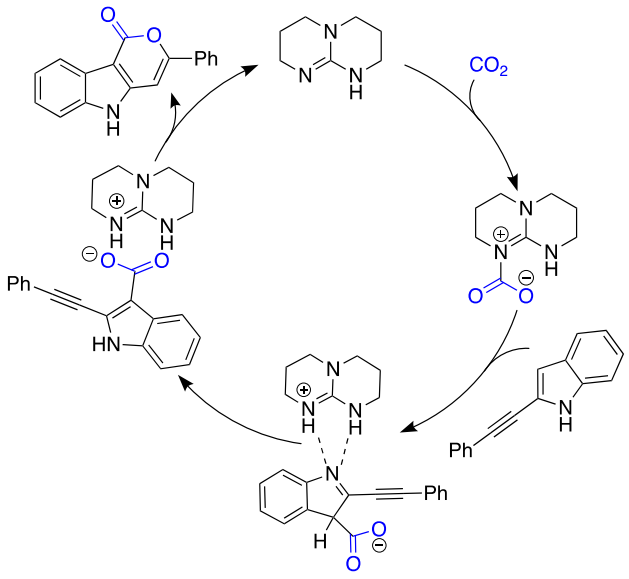

Figure 1.18. Catalytic cycle of CO_2 trapping reaction proposed by *Skrydstrup* et al.

This work is currently the best example of a catalytic CO_2 sequestration reaction. The reaction is capable of reaching >95% yield with only a threefold molar excess of CO_2 injected into an argon atmosphere, demonstrating that the system is adept at capturing CO_2. It proceeds under relatively mild temperatures and pressures which are well within reach for safe and sustainable process development. In addition, the products of this reaction have been tested and shown to inhibit human cervix adenocarcinoma cell growth[18], demonstrating the concept of "value-added" CO_2 sequestration. However, the proposed catalytic cycle shown seems a bit simplistic. The authors assert the importance of the TBD:CO_2 adduct as an on-cycle intermediate only with reference to other works which invoke similar species, and do not present any experimental evidence for this themselves. As discussed previously in this section, these base:CO_2 adducts may be inert, active, or even catalytic in CO_2 sequestration reactions. In addition, the lack of any computational or kinetic data leaves open the potential existence of more or different intermediates, and different rate orders in substrate, catalyst, or even CO_2. In addition, there is no discussion of why TMG and iPr*, which are competent CO_2 sequestration reaction catalysts in

other systems, do not perform well here. For all of these reasons, this particular work seemed like the best place to begin on the path towards furthering the current understanding of CO_2 activation and sequestration chemistry. The work in the following three chapters details the mechanistic, kinetic, and computational study of this reaction.

2. Experimental Studies:

2.1 Introduction:

A recurring theme in research published on CO_2 fixation that involves nitrogenous base catalysts is the invoking of a base:CO_2 adduct as an active species in the proposed mechanisms.[9,10,11] Due to the significance this assertion has in the modelling and understanding of the mechanism of catalysis in these reactions, further study of the nature of these species is warranted. In their report on the organocatalytic CO_2 trapping with alkynylindoles, Skrydstrup *et al.* suggest that a TBD:CO_2 adduct represents an "activated" form of CO_2 and is an on-cycle species in the reaction. Their proposed catalytic cycle is shown in Figure 2.1.

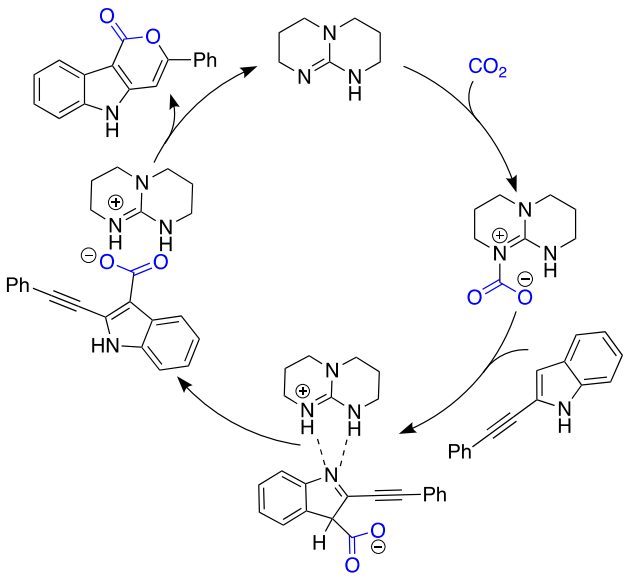

Figure 2.1. Catalytic cycle of CO_2 trapping reaction proposed by *Skrydstrup* et al.

However, upon investigation of the literature catalyst scope table there are two interesting discrepancies, shown in Table 2.1. First, the N-heterocyclic carbene (NHC) IPr* was tested as a catalyst and found to afford no conversion under literature conditions. IPr* is known to readily form a zwitterionic CO_2 adduct (Figure 2.2), which suggests that this ability is not the only determining factor of catalytic activity.[11] Second, DBU was found to promote this reaction well,

but has been shown to be incapable of forming a CO_2 adduct. DBU:CO_2 adducts have been invoked in organocatalytic CO_2 trapping reactions in the past[10], but *Franco* et al.[19] showed that these species actually consisted of monomeric and dimeric bicarbonates which formed from trace water included in solvents, and were not formally adducts analogous to the ones formed by compounds like TBD and IPr*.

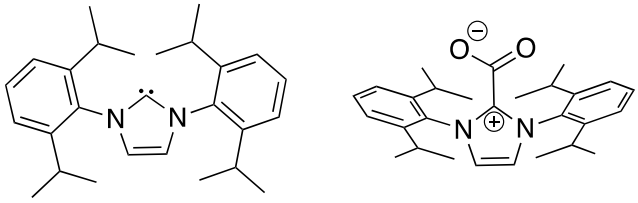

Figure 2.2. IPr* as free carbene and as its CO_2 adduct.

Catalyst	Forms CO_2 Adduct?	Promotes Reaction?[9]
TBD	Yes	Yes
IPr*	Yes[3]	No
DBU	No[4]	Yes

Table 2.1. Selected entries from the catalyst scope table of *Skrydstrup* et al. assessed for catalytic activity and ability to form stable CO_2 adducts.

These two discrepancies reveal the need to scrutinize the nature of the TBD:CO_2 adduct in this reaction. From only these entries in the scope table of *Skrydstrup* et al. it is reasonable to suspect this adduct might not actually be an active species in the reaction pathway. To probe this assertion, the specific behaviour of the adduct under reaction conditions was investigated. *in-situ* FT-IR monitoring was used to study the effect of different temperatures and pressures on the adduct in different solvents, specifically to see if there was any difference in equilibrium populations of reactant and products following Figure 2.3.

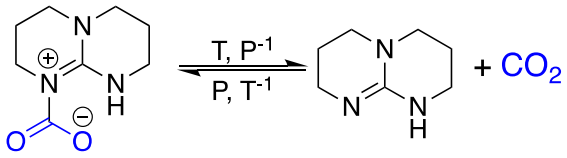

Figure 2.3. Reaction scheme depicting the TBD:CO_2 adduct in equilibrium with free base and CO_2. The equilibrium is shifted towards free CO_2 and TBD as pressure decreases and as temperature increases.

2.2 Physical Study of TBD:CO_2 Adduct:

As the literature conditions of the Skrydstrup *et al.* CO_2 trapping reaction make use of acetonitrile, and the kinetic studies reported herein are performed in diethylene glycol dimethyl ether (diglyme), the behaviour of the adduct in each solvent was compared. In addition, the study was also performed in DMSO and 1,2-dichloroethane to provide more data points for further comparison, which are shown in Table 2.2.

Solvent	**TBD:CO_2 Decomposition Temperature (°C)**
1,2-dichloroethane	35
Diglyme	85
Acetonitrile[a]	>110
Dimethylsulfoxide[a]	>125

Table 2.2. Decomposition temperature of TBD:CO_2 adduct in different solvents at 170 kPa CO_2. [a]-Experiment was stopped before decomposition was observed.

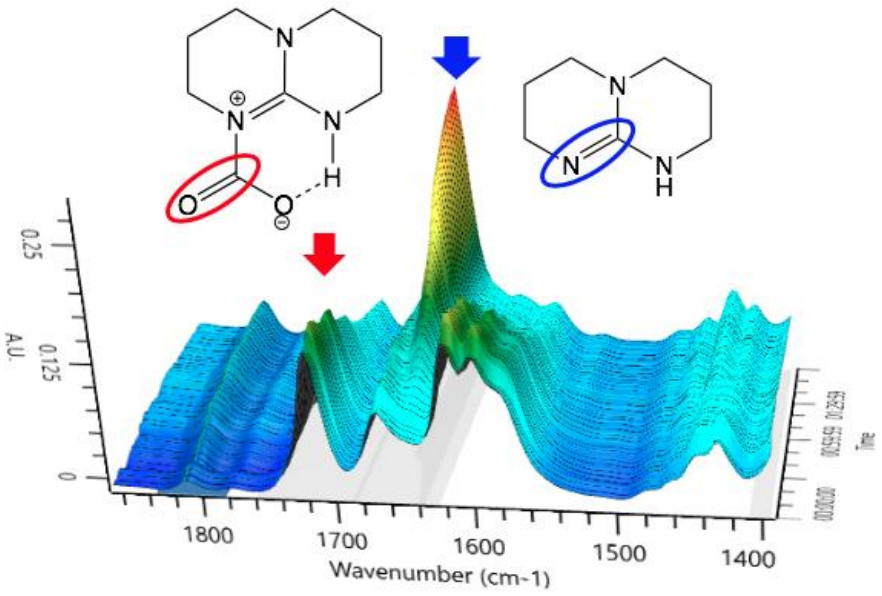

Figure 2.4. Waterfall FT-IR plot of TBD:CO_2 adduct thermal stability study in 1,2-dichloroethane with peaks of interest labelled and assigned following Nguyen *et al.*[19]

To perform these experiments a solution of TBD (0.2 M) in the dry, degassed solvent of interest was added to a Schlenk tube fitted with the FT-IR probe and a CO_2 inlet line. The pressure and temperature of the solution were incrementally varied, and the FT-IR spectrum of the solutions constantly monitored. Interestingly, the TBD:CO_2 adduct is quite stable in acetonitrile under reaction conditions (100 °C, 170 kPa), while in diglyme the adduct rapidly decomposes at about 85 °C and does not exist significantly under the reaction conditions.

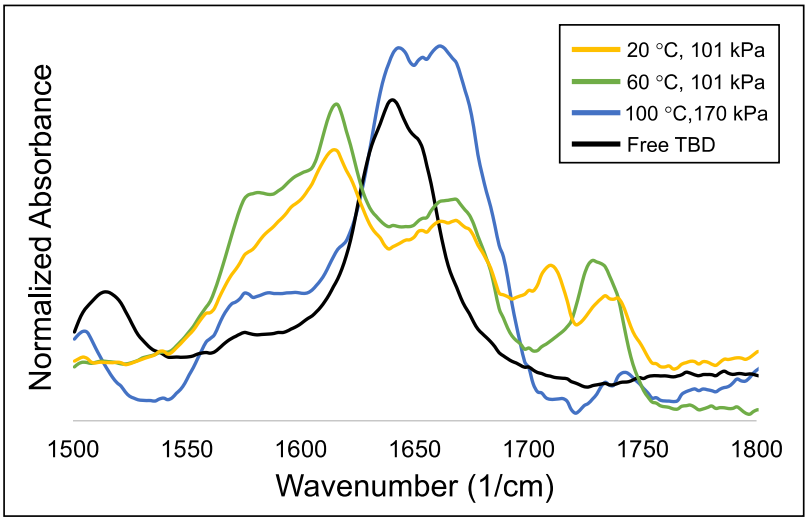

Figure 2.5. Normalized FT-IR spectra of TBD:CO_2 adduct in diglyme at various temperatures and pressures.

The formation of the adduct is monitored by the presence of the characteristic C=O stretch of the carboxylate at ~1720 cm^{-1}, whereas free TBD is indicated by the C=N stretch at ~1650 cm^{-1} as demonstrated in Figure 2.4. Furthermore the adduct is soluble in acetonitrile, but is insoluble in diglyme and is initially observed forming as a flocculent white precipitate. This suspension rapidly clears upon heating past 85 °C with some effervescence, indicating a sudden shift of the equilibrium towards free base and CO_2. The adduct showed very high thermal stability in DMSO, while decomposing quickly in DCE. This adduct stability data correlates in part to the dielectric constant of the solvent tested, which is a specific measure of solvent polarity. However DCE is more polar than diglyme by this measure which suggests that additional factors, such as Lewis basicity, must have an effect on this system.

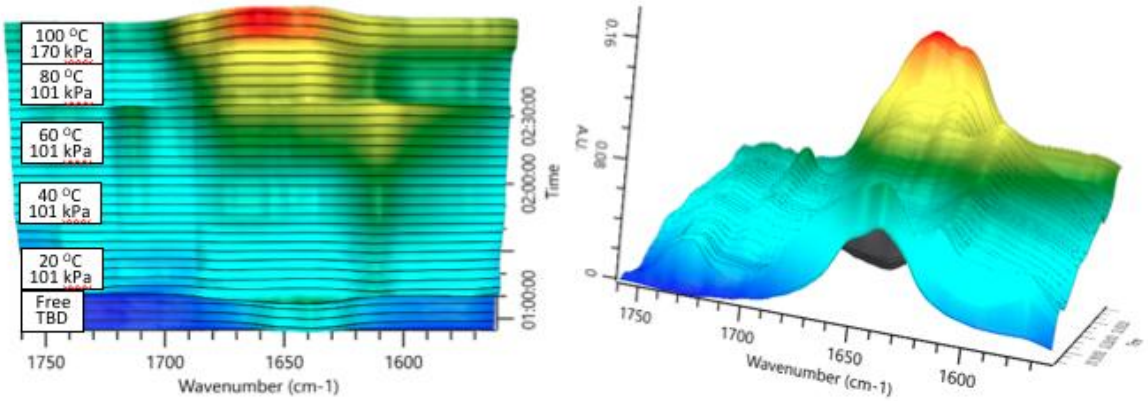

Figure 2.6. Overhead and side-on view of crude waterfall FT-IR plot of TBD:CO_2 adduct thermal stability study in diglyme at various temperatures and pressures.

Interestingly, the design of this series of experiments revealed a limitation of the *in-situ* FT-IR technique; the effect of thermal response. Because the adduct decomposes at such a low temperature in DCE (~35 °C), this experiment was conducted simply by slowly increasing the temperature of the solution until decomposition occurred, and the data shown in Figure 2.4 only represents a change in temperature of about 15 °C. However, in the case of the diglyme experiment shown in Figures 2.5 and 2.6, the effect of thermal response over the 80 °C range causes the baseline at the back of the waterfall plot to rise significantly above the front. This effect leads to data sets which are visually much more convoluted, and not as immediately intuitive. In addition, the effect of thermal response limits the quantitative use of this technique for any reactions which are not occurring under isothermal conditions.

2.3 Mechanistic Studies of TBD:CO_2 Reactivity:

While this physical study can't discount the potential for a very minor equilibrium population of the adduct in diglyme at 100 °C, there is a significant discrepancy between the adduct stability in diglyme and acetonitrile under the reaction conditions. This finding, combined with the inconsistency of the scope of catalysts to be able to both form CO_2 adducts and promote the

reaction (Table 2.1), goes a long way towards implying that a base:CO_2 adduct is not an on-cycle species in this reaction. Nevertheless, a series of mechanistic studies were performed in an effort to determine if the TBD:CO_2 adduct could react with the substrate under varying conditions. For these tests the substrate 2-phenylethynylindole (**2-PEI**) was chosen due to good performance and ease of synthesis. First, a background reaction was performed to test the ability of the literature reaction to proceed at ambient temperature, which indicated trace reactivity as shown in Figure 2.7. Observing reactivity in this control experiment suggested that similar reactivity between the adduct and **2-PEI** would occur at this temperature if the species do indeed react with each other.

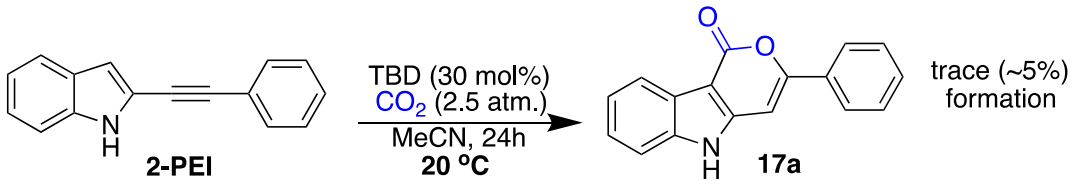

Figure 2.7. Control CO_2 trapping reaction performed at ambient temperature.

Next, a series of reactions were performed which involved combining the TBD:CO_2 adduct and **2-PEI** under varying conditions in an effort to afford reactivity, following the scheme of Figure 2.8. Throughout these tests air and water were thoroughly excluded to avoid formation of free CO_2 through adduct hydrolysis or introduction of trace CO_2 from the atmosphere.

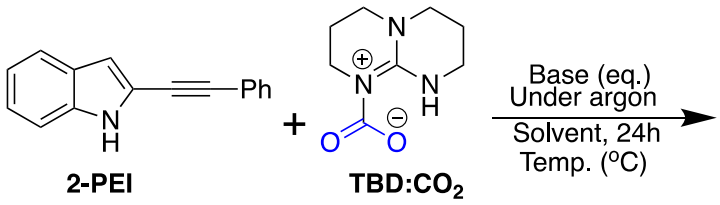

Figure 2.8. Reaction scheme for the test of TBD:CO_2 reactivity with **2-PEI** shown in Table 2.3.

Entry	Solvent	Base (eq.)	Temp (°C)	17a Yield
1	MeCN	-	20	N.R.
2	MeCN	-	60	N.R.
3	MeCN	TBD (1)	20	N.R.
4	MeCN	TBD (1)	60	N.R.
5	Diglyme	-	20	N.R.
6	Diglyme	-	60	N.R.
7	Diglyme	TBD (1)	20	N.R.
8	Diglyme	TBD (1)	60	N.R.
9	Diglyme	-	100	~25%
10	MeCN	-	100	Trace (<3%)

Table 2.3. Scope of conditions tested in the reaction of TBD:CO_2 adduct with **2-PEI**. All reactions performed on a 0.1 mmol scale in dry, degassed solvent under argon for 24 h.

Initially, **2-PEI** and TBD:CO_2 were combined in equimolar ratio in acetonitrile and left to react at ambient temperature. When no reaction was indicated by ^{1}H NMR or TLC after 24 hours, the mixture was heated to 60 °C and stirred for a subsequent 24 hours, after which time product formation was still not observed. This process was repeated in diglyme, which gave the same results. Next **2-PEI**, TBD:CO_2, and free TBD were combined in equimolar ratio in acetonitrile to determine if both the adduct and free base are necessary for this reaction. The mixture was stirred at room temperature for 24 hours which again afforded no product formation. The heating process was repeated again to the same result, as were the subsequent equivalent tests with free TBD in diglyme. Interestingly, and in line with the findings from the *in-situ* FT-IR study, is the reaction shown in entry 9. When an equimolar combination of TBD:CO_2 and **2-PEI** was stirred at 100 °C for 24 hours in diglyme, the reaction proceeded significantly. The IR data presented previously shows the adduct is not stable under these conditions, and it can be reasoned that the reaction proceeded as the adduct broke down into free CO_2 and TBD. When the same reaction was performed in acetonitrile, only trace formation of the product was observed. These relative rates of reaction are consistent with the data collected pertaining to the thermal stability of the TBD:CO_2

adduct in these two solvents, although this does show some minor equilibrium concentration of free TBD and CO_2 exists in acetonitrile at 100 °C. From this series of experiments it can reasonably be concluded that the TBD:CO_2 adduct combining with **2-PEI** to afford **17a** is not the preferred pathway of this reaction. Skrydstrup *et al.* propose the TBD:CO_2 adduct is an activated form of CO_2 which can be directly attacked by **2-PEI**. Under the varying conditions of this experimental study, this claim could not be substantiated.

There is an interesting and specific mechanistic insight which is derived from comparing entry 10 in Table 2.3 with the literature reaction conditions, as shown in Figure 2.9.

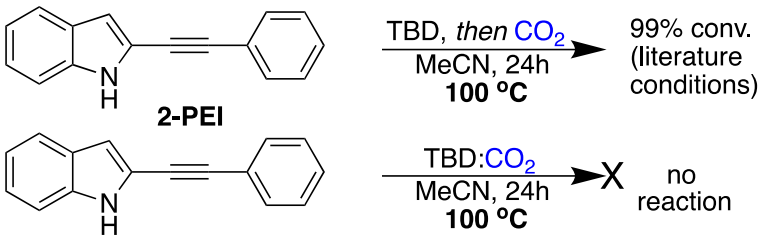

Figure 2.9. Different reactivity of 2-PEI with TBD and CO_2 depending on order of addition of the compounds.

In their work, Skrydstrup *et al.* optimize their reaction to proceed using only 3 eq. CO_2 injected into the sealed reaction vessel containing the rest of the reaction mixture, which was previously loaded into the vessel in a glove box. The vessel is removed from the glovebox prior to CO_2 addition. This procedure leads to a 90% yield over 20 hours with **2-PEI**. The important detail of the experimental procedure of Skrydstrup *et al.* is this: under literature conditions the TBD and **2-PEI** are combined at least a *few minutes prior* to the addition of CO_2 to the reaction vessel. The *in-situ* FT-IR study of the TBD:CO_2 adduct shows that the equilibrium population of the adduct in acetonitrile at 100 °C is very high. Reaction 10 in Table 2.3 shows that the reaction between TBD:CO_2 and **2-PEI** in acetonitrile at 100 °C proceeds only slightly. These two experiments, when compared in the context of the literature reaction procedure, suggest that **2-PEI** inhibits the formation of the TBD:CO_2 adduct in some way. Whether or not TBD formally deprotonates

2-PEI, the two molecules are clearly strongly associated before CO_2 is added to the reaction mixture. These studies show that if all of the TBD present in the reaction mixture were to immediately form the CO_2 adduct upon its addition, the reaction would not proceed significantly. Rather, following the literature procedure the formation of the TBD:CO_2 adduct is not favourable.

As some researchers have asserted that the competency of a catalyst to facilitate CO_2 trapping reactions is directly related to basicity[12,19], a reaction using a strong, irreversibly-deprotonating base was conducted in a final attempt to afford reactivity between the **2-PEI** substrate and the TBD:CO_2 adduct. To this end, **2-PEI** was combined with sodium hydride in acetonitrile and stirred for 30 minutes before the introduction of 1.2 eq. TBD:CO_2 as shown in Figure 2.10.

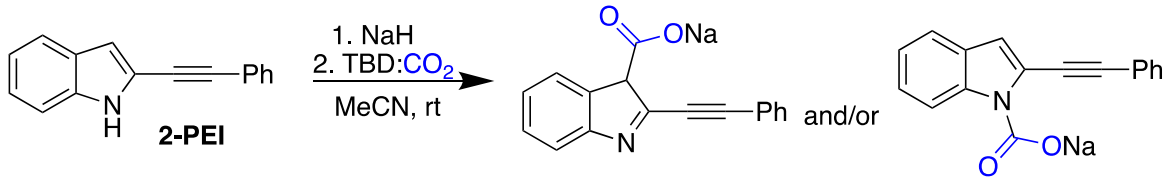

Figure 2.10. Reaction scheme for the combination of [Na^+][2-PEI^-] and TBD:CO_2 adduct in acetonitrile showing potential intermediate products.

Upon workup with saturated ammonium chloride solution only the starting material was recovered, with no indication of any carboxylated products by ^{1}H NMR. Based on this result the role of the TBD:CO_2 adduct as an on-cycle intermediate was discounted, and focus was turned to other mechanistic details.

2.4 Other Mechanistic Studies:

Next, the nature of the indole N-H bond was considered. TBD, being very strongly basic, could potentially deprotonate this position and inductively activate the substrate as a nucleophile. To test this hypothesis, 1-methyl-2-phenylethynylindole (**22**) was synthesized and subjected to the literature reaction conditions as in Figure 2.11.

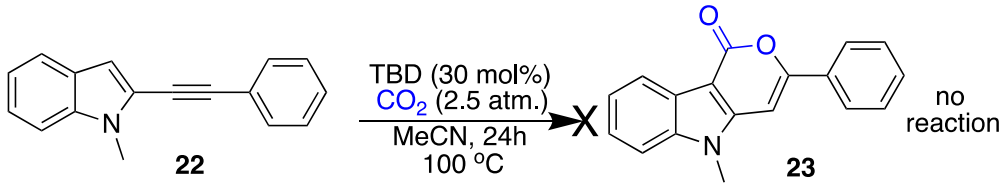

Figure 2.11. Scheme for the reaction of N-methyl 2-PEI with TBD and CO_2 following literature reaction conditions, which gave only starting material.

Here, the formation of the new species **23** would have provided a new N-methyl ^{1}H NMR signal and a reduction in the integration value of the 3-position signal, which was not observed. In addition, the reaction mixture remained unaltered with respect to the starting material by TLC analysis. This experiment shows the necessity of the indole 1-proton for this transformation to occur, however no conclusions about the role of this proton can be drawn. It was subsequently hypothesized that the deprotonation of **2-PEI** could be necessary to activate TBD as a catalyst, and not to activate the substrate as a nucleophile, which could potentially occur by allowing TBD to more strongly coordinate CO_2 in the cationic protonated state. To test this hypothesis, the tetrafluoroborate salt of TBD (which is actually an ionic liquid) was synthesized and tested for catalytic activity with **22** as shown in Figure 2.12. Tetrafluoroborate was chosen as it is a weakly coordinating anion and is unlikely to influence the reaction while facilitating the solubility of the salt in acetonitrile.

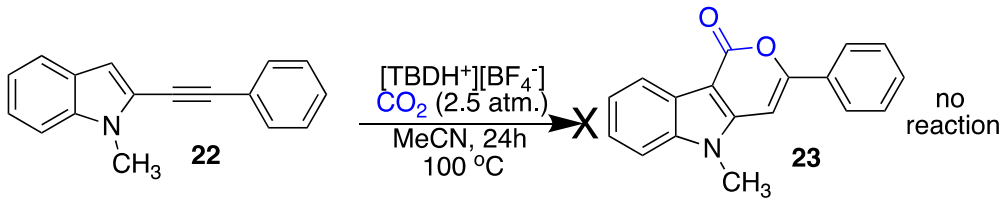

Figure 2.12. Scheme for the reaction of a protonated TBD salt with 1-Me-2-PEI under literature conditions, which gave only starting material.

This reaction did not afford any of the expected product **23** by ^{1}H NMR or TLC analysis, which rules out the role of the indole N-H proton as a simple catalyst activator. This protonated TBD salt was also tested for catalytic activity on the literature substrate **2-PEI** as shown in Figure 2.13.

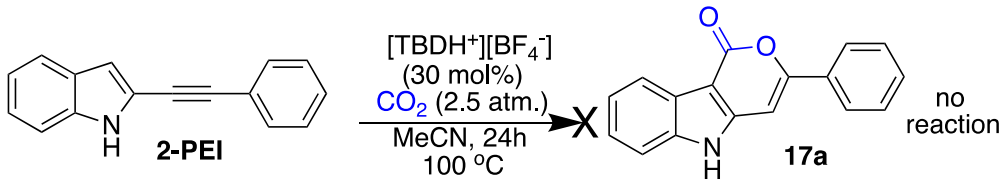

Figure 2.13. Scheme for the reaction of a protonated TBD salt with 2-PEI following literature reaction conditions, which gave only starting material.

No reaction was observed under these conditions either, which further suggests that the deprotonation of the substrate at some point in the reaction by the TBD catalyst is important. As a final test, **2-PEI** was simply deprotonated with sodium hydride in acetonitrile at ambient temperature and the solution was pressurized with CO_2, shown in Figure 2.14. This also afforded only the starting material and no **17a** upon workup.

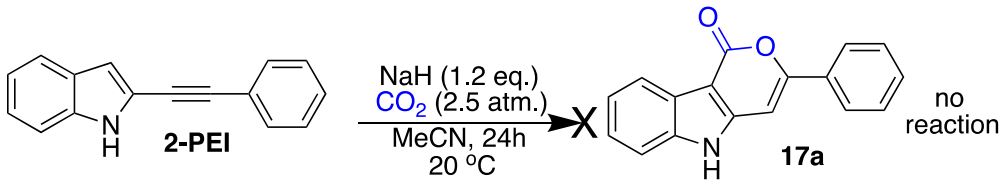

Figure 2.14. Scheme depicting the reaction of 2-PEI with sodium hydride and CO_2 in acetonitrile at ambient temperature. This reaction afforded only starting material upon analysis.

2.5 Conclusions:

These mechanistic studies collectively reveal numerous different aspects of this reaction. First, the TBD:CO_2 adduct does not appear to be an on-cycle intermediate in the catalytic cycle, and may or may not be present during the reaction to little effect. While the physical chemical FT-IR study can't discount a minor equilibrium population of the adduct existing in diglyme under the reaction conditions, no efforts to afford direct reaction between this adduct and **2-PEI** were

successful. Next, the importance of the substrate N-H bond has been demonstrated. The N-methylation of the substrate completely stops this transformation from taking place. Since both the starting material and the product in this reaction possess the indole N-H bond, it seems as if this bond must break and then reform during the course of this reaction. Finally, the role of this N-H bond lies beyond simply being deprotonated, whether to activate the substrate as a nucleophile or to activate TBD as a catalyst. The exact mechanism of this transformation cannot be determined from simple mechanistic studies, however a few specific aspects of the mechanism of catalysis have been revealed through them. TBD is certainly a multifunctional catalyst in this reaction; as a coordination catalyst, a base, and subsequently as a proton shuttle all together.

3. Kinetic studies:

As discussed in the previous section, the existing model of catalysis for the Skrydstrup reaction is incompatible with the presented experimental findings. For this reason, a kinetic profile of this reaction was developed to better understand the mechanism of catalysis at hand. Kinetic studies are extremely powerful tools that are used to further understand the nature of chemical systems through the careful use of specific experimental design. Information pertaining to the specific properties of a system of reactants and products can be found through the control of experimental variables, the most common being concentration and temperature, however others such as pressure and rate of mixing are also studied. Physical data such as rate orders, rate constants, and catalytic activity are all experimentally determined through kinetic studies. Through the kinetic profiling of the Skrydstrup reaction, the understanding of the catalytic mechanism through which the reaction proceeds can be expanded.

Initially, some modification of the literature conditions was necessary to make this reaction more amenable to safe and effective study. As this reaction proceeds above the boiling point of acetonitrile at atmospheric pressure, the use of a different solvent with a higher boiling point was desirable for the bulk of the kinetic studies as a safety measure. In addition, an experimental apparatus was designed to deliver constant CO_2 pressure across two different reaction mixtures concurrently to reliably collect data in duplicate. To monitor the progress of the reaction a chromatographic method was developed using supercritical fluid chromatography- ultra-high-pressure liquid chromatography (SFC-UHPLC). Separation was performed on a 1260 Infinity II HPLC (Agilent, Santa Clara, USA) using a 150x 4.6 mm Zorbax RX-SIL column (Agilent, Santa Clara, USA). Samples were eluted using a gradient elution method with CO_2 and iPrOH and analyzed for absorbance at 254 nm using a diode array detector (DAD). The mobile phase was

pumped for 10 minutes with 95:5 CO_2:iPrOH, and then for 20 minutes with 85:15 CO_2:iPrOH at 0.5 mL/min. HPLC-grade isopropanol was purchased from Sigma-Aldrich (St. Louis, USA) and used as obtained. Naphthalene was used as an internal standard and was recrystallized from ethanol prior to use. A standard curve was used to ensure the response factor of **2-PEI** was linear within experimentally relevant concentrations and is shown in Figure 3.1.

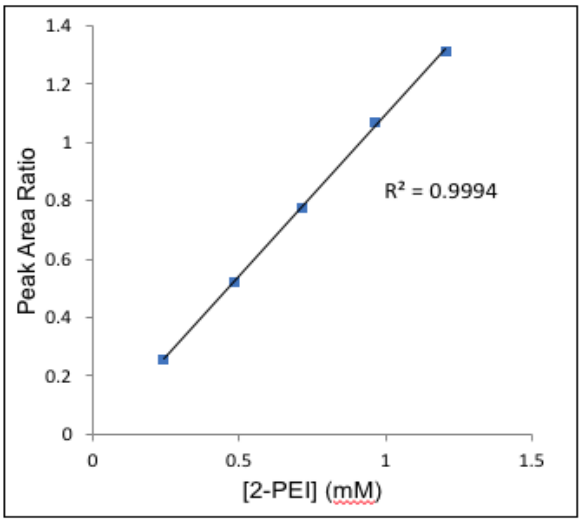

Figure 3.1. Standard curve showing change in integrated peak area ratio of naphthalene to 2-PEI as a function of differing 2-PEI concentration.

From the ratio of integrated peak areas of naphthalene and **2-PEI**, and the known starting concentration of **2-PEI**, the concentration of **2-PEI** is calculated at every sample point using the following equation:

$$(1)\quad [X]_T = [X]_0 * \frac{(Peak\ Ratio)_T}{(Peak\ Ratio)_0}$$

where $[X]_T$ and $[X]_0$ represent the concentration of **2-PEI** at a sample point and at the start of the kinetic study, respectively.

Kinetic data was obtained for the CO_2 trapping reaction at 10, 20, and 40 mol% TBD catalyst. Kinetic experiments were performed in duplicate at each catalyst concentration both for time efficiency and to ensure that all relevant concentrations were as identical as possible. At time

t=0:00 the reaction mixtures containing **2-PEI**, TBD, and naphthalene dissolved in diglyme were transferred via syringe into the reaction vessels. The vessels were previously equilibrated to 100°C and the experimental CO_2 pressure of 10 psi (170 kPa). The pressure was reduced from the literature conditions as a safety consideration. Following this, at each time point, small aliquots were removed via syringe and analyzed by SFC-UHPLC, giving the raw data shown in Figure 3.2.

Despite the challenging experimental design of this kinetic study, the data obtained across different runs at a set catalyst loading is in close agreement. Here, the relatively larger run-to-run variance in the 40 mol% experiments is simply a result of the reaction proceeding more quickly, which magnifies the inherent error in the method.

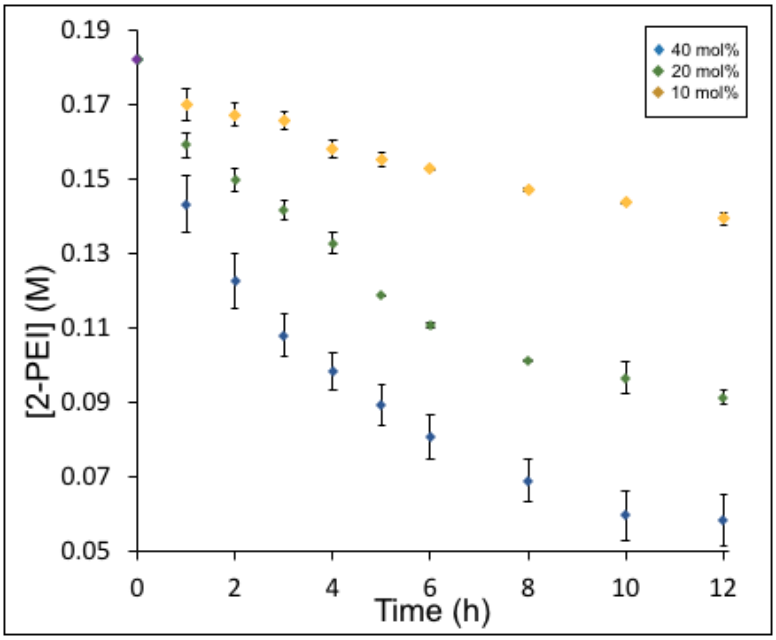

Figure 3.2. Raw kinetic data representing the averages of multiple runs at different catalyst loadings with error bars showing standard deviation.

From this data the average rate of each reaction was analyzed graphically by plotting the rate of starting material consumption as a function of time for each different catalyst loading.

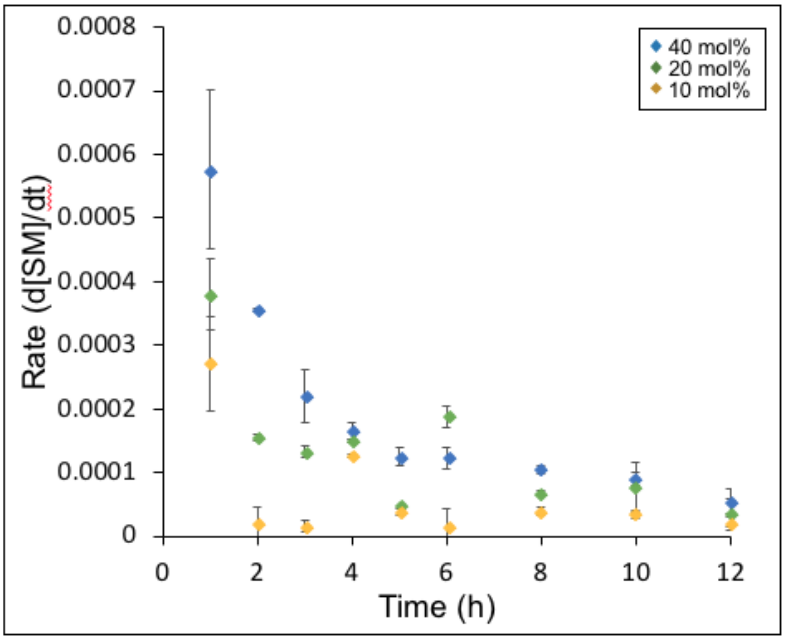

Figure 3.3. Rate of substrate consumption as a function of time for each catalyst loading tested. This data represents the averages of 2, 2, and 3 runs for 10, 20, and 40 mol%, respectively.

As one of the components of this reaction (TBD) is only present in catalytic amounts, the typical method of graphical analysis by fitting the raw data to ln[SM] or -1/[SM] cannot be used for rate order determination. As Figure 3.3 shows some very odd kinetic behaviour, analysis of the catalyst rate order in this reaction is conceptually split into two parts which reflect the kinetic profile. The initial rate order is determined through the relationship of initial rate to catalyst concentration for each catalyst loading. In this study, the initial rate is taken as the amount of substrate consumed in the first hour of the reaction.

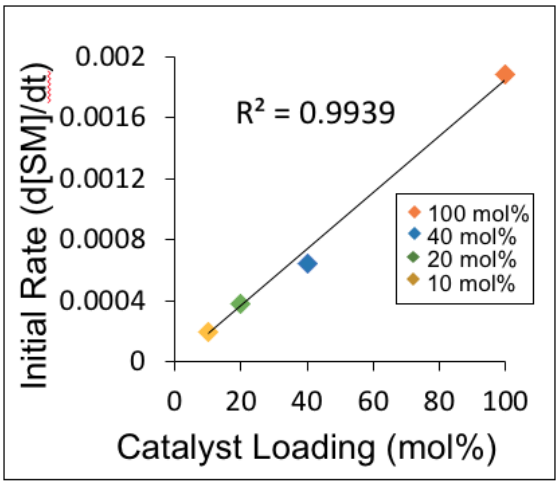

Figure 3.4. Plot showing the linear fit of initial reaction rate to the catalyst loading added to the reaction mixtures. Data for the 100 mol% initial rate represents the average of two runs.

Figure 3.4 shows the linear fit of initial rate values to the mol% of catalyst used in each reaction, indicating that the reaction is initially first order in TBD. Were this reaction to be initially second order an exponential fit would be expected, with a doubling in catalyst loading giving a four-fold increase in reaction rate. Similarly, an initial rate order of zero would manifest as initial rates independent of catalyst loading. The initial rates of the catalytic (10, 20, and 40 mol%) run averages increase linearly with catalyst loading, but because initial rate analysis is not limited to substoichiometric catalyst loading a 100 mol% initial rate is also included as an extra data point.

After determining the initial rate order of TBD is one in the reaction, attention was turned to the analyzing the kinetic profile of the rest of the reaction. As seen in Figure 3.2, there is an obvious anomaly in the kinetic profile of the reaction visible at the four-hour mark. Taking a closer look at the raw kinetic data for the 10 and 20 mol% catalyst loading runs in Figure 3.5 gives some insight into what may be occurring here.

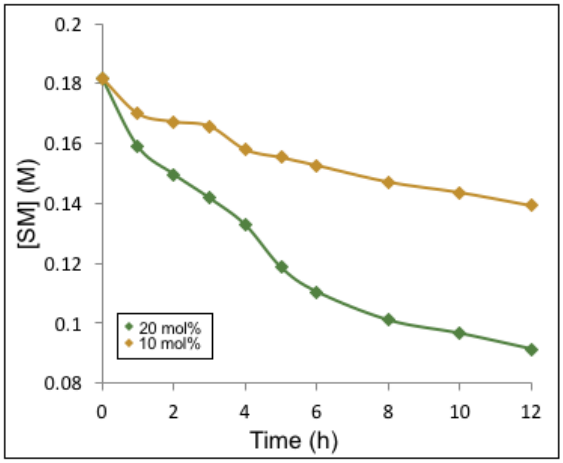

Figure 3.5. Magnified version of raw kinetic data of 10 mol% and 20 mol% runs showing potential plateauing effect. Experimental points connected for the sake of clarity.

Figure 3.5 demonstrates that the reaction proceeds initially in a first order manner but then exhibits a change in behaviour, after which time the substrate is consumed in a linear fashion with respect to time, indicating a shift to zero-order behaviour. While chemical reactions which have changing kinetic profiles are not uncommon, a thorough analysis and explanation of this particular effect must be performed. While the 40 mol% runs do not have an appreciably visible plateauing effect, they do share a common artefact with the runs at other concentrations; the time to complete one turnover.

TBD (mol%)	TBD (M)	TON at 3h
40	0.07272	1.01
20	0.03636	1.03
10	0.01818	0.99

Table 3.1. Turnover number of TBD at t=3h for each catalyst loading, showing close agreement between the values over different catalyst loadings.

Table 3.1 shows that this change in reaction rate order is immediately preceded by one catalyst turnover. The likely mechanistic implication of this result is that the resting state of the catalyst changes after there is a molar equivalent of the reaction product present in solution. This effect is

due to the much greater acidity of the product **17a** relative to **2-PEI** in this reaction and is discussed in detail in the following section.

After determining the kinetic profile of the reaction in diglyme, it was endeavoured to attempt a single set of runs in acetonitrile under the same conditions to verify similar rate order behaviour. Working cautiously with a modified apparatus, single experiments at 20 and 40 mol% TBD loading were performed under the same experimental conditions as the previous runs.

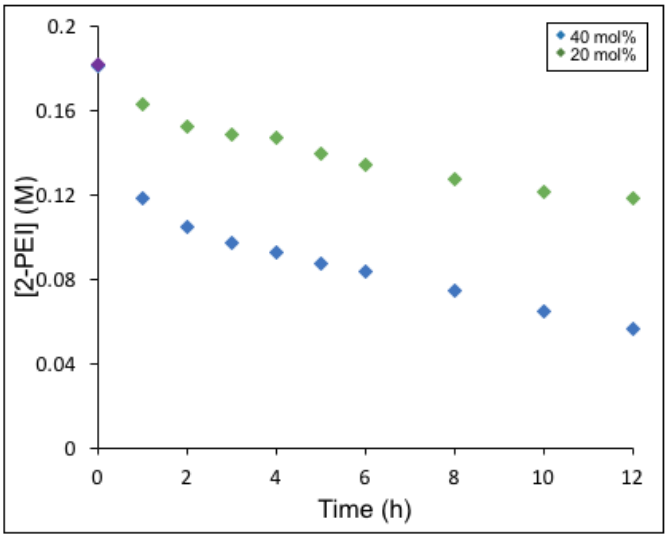

Figure 3.6. Raw kinetic data obtained from single experiments at 20 and 40 mol% catalyst loading in acetonitrile.

This data is then treated the same way as that obtained from the diglyme experiments, with rate as a function of time plotted for each catalyst concentration shown in Figure 3.7.

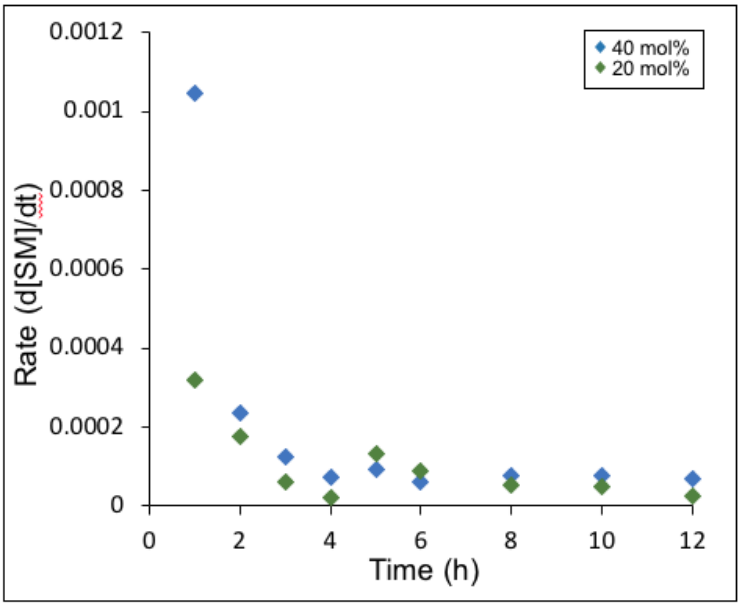

Figure 3.7. Rate of substrate consumption as a function of time for each catalyst loading tested in acetonitrile.

As Figure 3.7 shows, the kinetic profile of this reaction in acetonitrile is in close agreement with the profile in diglyme, which is shown in Figure 3.3. In acetonitrile, the change in kinetic behaviour of the reaction is more obvious, with a rapid decrease in reaction rate occurring up to t=4h, after which time the rate plateau is very obvious. Interestingly, analysis of the reaction in both solvent systems shows the same peculiar behaviour, where there is a marked increase in rate around the t=4-6h mark. While this isn't visible in diglyme at 40 mol%, it can be observed in the acetonitrile reaction system. Although unlikely, it is possible that the mechanism of the reaction could change between solvents as acetonitrile is significantly more polar than diglyme (MeCN ε = 36.64, diglyme ε = 7.23)[20]. However, the data obtained shows that the rate behaviour of the reaction is consistent between the two solvents, being initially first order before plateauing after one catalyst turnover. As the literature reaction conditions stipulate the use of acetonitrile as the reaction solvent, the ability to show that the kinetic behaviour remains the same in diglyme is vital for the assertion that the overall reaction mechanism has not changed as a result of switching solvents. The kinetic data presented herein is next used for the informed construction of a computational

model of this reaction in the next chapter of this work. Further, revealing this unique catalyst behaviour will further the understanding and development of CO_2 trapping reactions using strong base catalysts.

4. Computational Modelling:

4.1 Model Development:

The final challenge in the study of the Skrydstrup *et al.* reaction was to develop a competent mechanistic model of the reaction guided by the specific details revealed by experimental study. The experimental work presented in the previous sections shows two specific incompatibilities with the literature catalytic cycle, which this modelling endeavours to correct. First, the mechanistic work presented herein discounts the feasibility of invoking a TBD:CO_2 adduct as an activated form of CO_2 in the catalytic cycle, demonstrating the need for modelling a different approach to CO_2 activation. Second, the demonstration of a shift from first to zero-order behaviour after one turnover necessitates a mechanism which is more complex than the literature proposal. This change in kinetic behaviour must be explainable by the proposed reaction model in order for it to be an accurate representation of the catalytic cycle. With this in mind, the concept of the tightly associated substrate-catalyst complex derived from the mechanistic work was taken as a conceptual starting point in creating the model of the reaction. In needing to develop a different model to explain CO_2 activation, and with the initial rate order in mind, a hydrogen-bonded supramolecular assembly in which TBD proximally coordinates the **2-PEI** substrate and a molecule of CO_2 was envisioned. In this model, the catalyst behaves as a coordinative activator of the system, bringing CO_2 and the substrate into the close proximity needed to react through hydrogen-bonding interactions.

The geometries of all structures were optimized at the B3LYP[21,22] level of theory using a 6-31g(d) basis set.[23,24] Following optimization of the structures, more intensive single-point (SP) calculations were performed to provide more accurate energies for comparison. These calculations were performed at the M062x[25] level of theory using a 6-311++g(d,p) basis set.[26] Calculations

were performed using a polarized continuum solvation model (PCM) with acetonitrile as the solvent. In these calculations the alkyne substituent of the substrate was modelled as a methyl group to ease the cost demand of the system. All calculations were carried out using the *Gaussian09*[27] package, and all structures were visualized using *GaussView 5.0*[28] software.

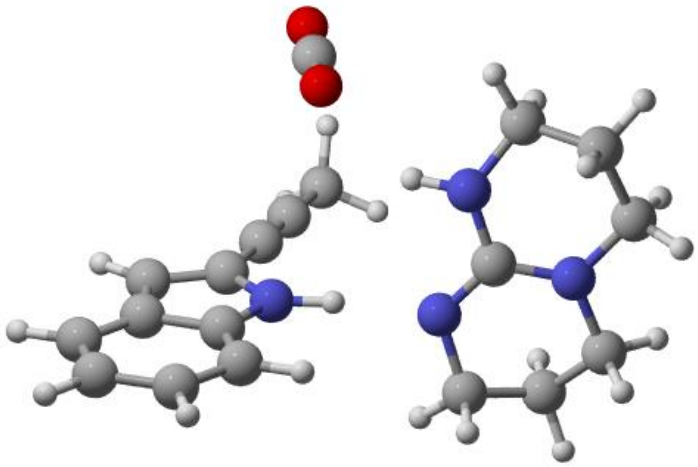

Figure 4.1. Optimized geometry of **SMa**, in which the TBD catalyst proximally coordinates the substrate and CO_2.

To evaluate the energetic feasibility of the starting material assembly (**SMa**) structure shown in Figure 4.1, the isodesmic equation comparing the energy of **SMa** to the energies of the three individual component molecules was solved. For this energy calculation the B3LYP optimized structure energies were compared, rather than the single-point energies. The M062x level of theory tends to give larger basis set superposition error (BSSE) than B3LYP in these types of energy comparisons due to the overestimation of hydrogen-bonding interaction energies.[29] Thus, while the M062x calculations are more accurate for comparing relative energies between different structures within the supramolecular assembly, the B3LYP calculations are more accurate for comparing the individual energies of each component to the larger structure.

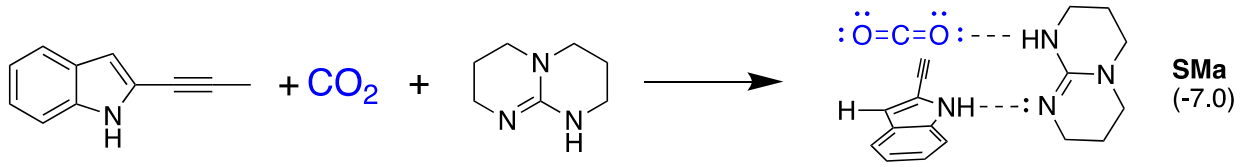

Figure 4.2. Isodesmic equation showing the favourability of **SMa** formation from its constituent molecules in acetonitrile. Relative Gibbs energies are given in kcal/mol.

The difference in energy between the starting materials and the supramolecular assembly arises from the establishment of two hydrogen bonding interactions, the energies of which can span two full orders of magnitude from 0.2-40 kcal/mol.[30] As a result, the three molecules in the **SMa** complex are held in close proximity by hydrogen bonding interactions, with intermolecular distances shown in Figure 4.3.

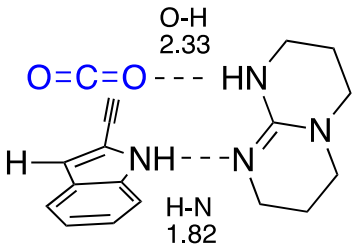

Figure 4.3. Hydrogen-bonding interactions in the **SMa** molecular assembly. Distances are given in Angstroms.

The N-H distance is quite short and is indicative of a very strong hydrogen bonding interaction. These interactions are facilitated by the high dielectric solvent acetonitrile, which is well suited to stabilize the buildup of charge that occurs as a result of these interactions.

Next, based significantly on the small N-H distance, the difference in energy between the neutral **SMa** complex and the ionic complex where TBD has deprotonated the indole-1 position was determined. As the mechanistic studies suggested that the indole N-H proton was necessary for the reaction, the difference in energy between these two species allows for analysis of how feasible the deprotonation step is.

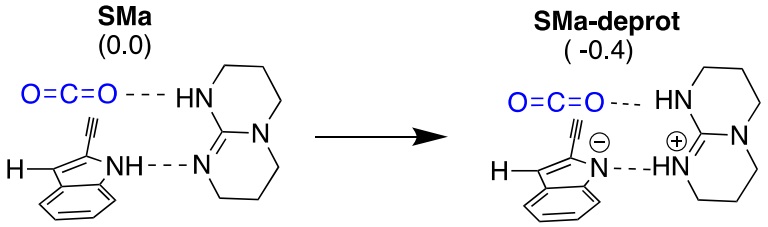

Figure 4.4. Relative Gibbs energies (kcal/mol) of **SMa** and the structure **SMa-deprot** which results from the deprotonation of the indole by TBD in **SMa**, showing the slight favourability of substrate deprotonation by TBD.

As demonstrated in Figure 4.4, the result of this energy comparison shows that the structure in which the indole N-H proton has been abstracted by TBD is mildly favourable. Interestingly, when the analogous energy comparison is made in the absence of CO_2 the deprotonation is no longer favourable, as illustrated in Figure 4.5.

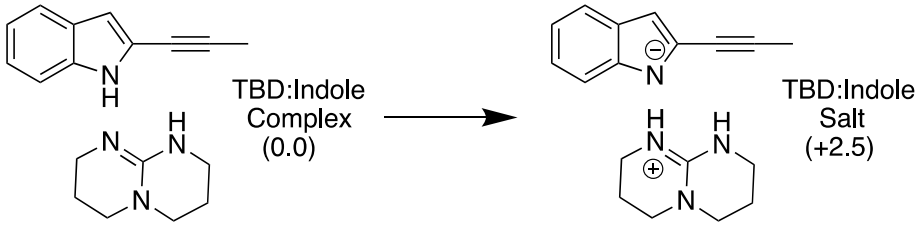

Figure 4.5. Relative Gibbs energies (kcal/mol) of the indole:TBD complex with and without proton transfer, showing the less favourable nature of the deprotonation in the absence of a CO_2 molecule.

Although these energy differences are relatively small, this result validates the proposed starting material assembly which was envisioned as a way to explain the reactivity of this system. In both of these models, substrate deprotonation occurs as the transfer of a proton along a preexisting hydrogen bond, and thus the resulting salts retain the same type and number of hydrogen bonding interactions. The energy difference in the **SMa** system resulting from the presence of CO_2 arises from the charge delocalization in the $TBDH^+$ cation, which causes the pre-existing N-H bond in TBD to become a stronger hydrogen bond donor towards the proximal oxygen atom of CO_2.

The next step in this model is the carboxylation of the indole-3 position, during which the multifunctional nature of the TBD catalyst manifests itself. After substrate deprotonation, the

$TBDH^+$ cation in **SMa-deprot** holds the substrate and CO_2 in a position which provides favourable orbital overlap for the C-C bond formation step. The carboxylation step proceeds with a transition state (**TS1**) barrier of 13.0 kcal/mol relative to **SMa**, giving the tetrahedral intermediate **Int1a** as shown in Figure 4.6.

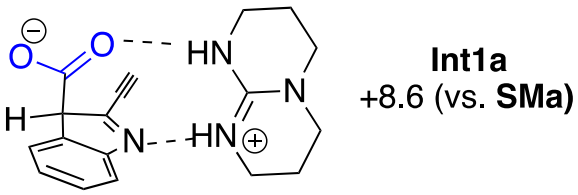

Figure 4.6. Structure of the intermediate resulting from the carboxylation of the indole-3 position of 2-PEI. Relative Gibbs energy is shown in kcal/mol.

Although substrate deprotonation in this model is favourable, it is also possible that the proton transfer and carboxylation steps of this reaction are concerted. The molecular assembly of **SMa** biases the system towards favourable orbital overlap for this to be the case, and the typical barrier to proton transfer along a pre-existing hydrogen bond between electronegative atoms is only about 1 kcal/mol, which would not significantly increase the transition state energy of this step.[31]

The next step of this reaction model involves the rearomatization of the indole moiety in the substrate through deprotonation at the site of carboxylation, which is the rate-determining step. A mechanistic step which involves reforming aromaticity and necessitates only the removal of a proton would usually be regarded as very favourable and with a low barrier to overcome. The reason this is not the case in this reaction model lies in the structure of **Int1a**. As the initial rate data obtained from kinetic experiments show that the rate determining step of this reaction is first order in catalyst, there can only be one TBD molecule present during this next step. However, upon formation of **Int1a** that one TBD molecule exists in its protonated form, which is not capable of deprotonating the indole-3 position. Before rearomatization of the indole can occur, the $TBDH^+$ cation must transfer its proton back to the substrate and convert back to the neutral base. This

process is extremely unfavourable and causes this step of the reaction shown in Figure 4.7 to be very slow.

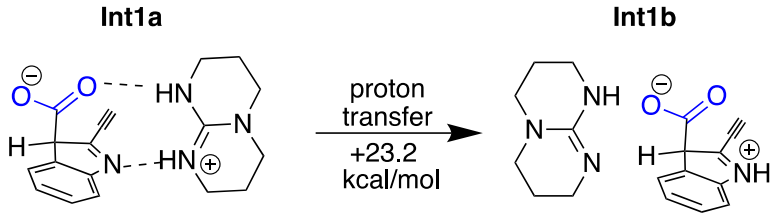

Figure 4.7. Structures of **Int1a** and **Int1b** showing the relative Gibbs energy difference between the two.

In fact, the resulting intermediate (**Int1b**) is so high in energy that the system has essentially overcome the transition state barrier to rearomatization when **Int1b** is formed. This is confirmed by the extremely similar structures of **Int1b** and **TS2**, which are shown in Figure 4.8.

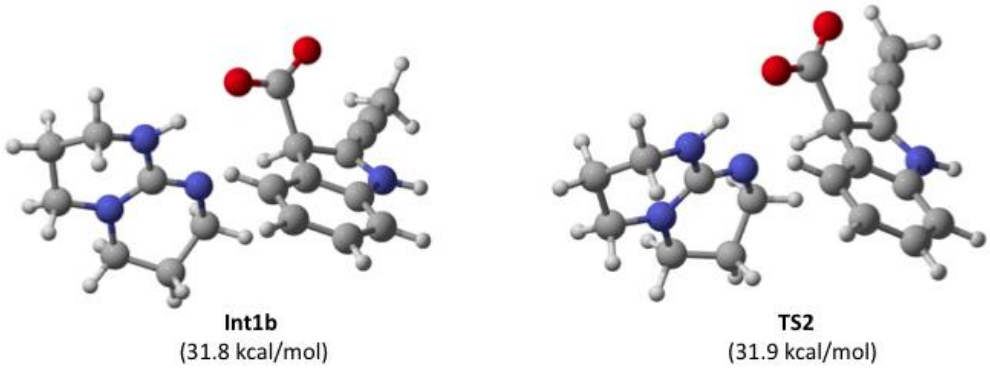

Figure 4.8. Structures and Gibbs energies (relative to **SMa**) of **Int1b** and **TS2**.

While having a high barrier, this rearomatization step is also quite exergonic, and **Int1b** proceeds to **Int2** with the release of 37.7 kcal/mol as shown in Figure 4.9.

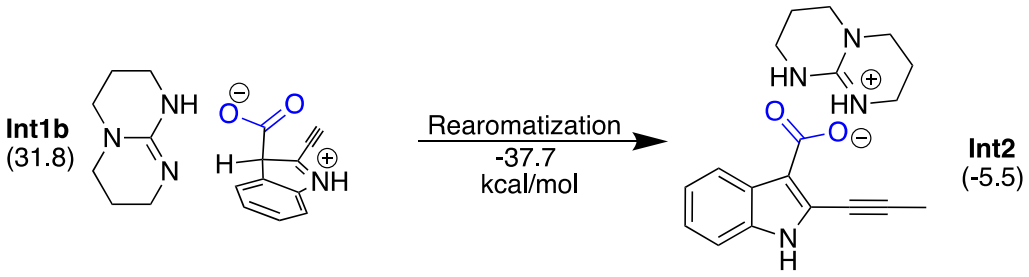

Figure 4.9. Formation of **Int2** from the rearomatization of **Int1b**, which is the rate determining step in this reaction model. Intermediate Gibbs energies (kcal/mol) are relative to **SMa**.

This step is so exergonic because it consists of three different energetic payoffs which occur simultaneously as **Int2** forms; re-establishing aromaticity in the indole moiety, the reformation of the stable $TBDH^+$ cation, and the favourable binding of this cation to the carboxylate anion of the intermediate.

Following the formation of **Int2**, the next and final energetic barrier is the transition state of the cyclization (**TS3**), which is 18.6 kcal/mol above **SMa**, or 24.1 kcal/mol above **Int2**. This step gives the penultimate intermediate (**Int3a**), which is 10.7 kcal/mol above **SMa**. Overall, the cyclization of **Int2** is 16.2 kcal/mol uphill, which is largely due to the formation of a carbanion in this step. Finally, **Int3a** is rearranged as TBD shuttles the indole N-H proton to the carbanion site, forming **Int3b**, which is 35.9 kcal/mol downhill, and represents the resting state of TBD after completing one reaction cycle. Overall, this reaction is exothermic, and 25.2 kcal/mol is released. This is summarized in Figure 4.10.

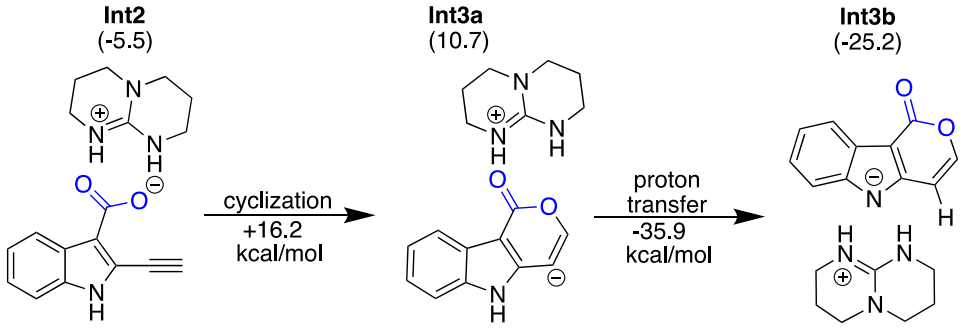

Figure 4.10. Structures of the final three reaction intermediates with Gibbs energies (kcal/mol) shown relative to **SMa**. The cyclization step has a transition state barrier (**TS3**) of 24.1 kcal/mol and the proton transfer step is assumed to have a negligible barrier.

Int3b contains the structure of the deprotonated product of this reaction, and when the $TBDH^+$ cation transfers a proton to the indole nitrogen free TBD and product form, and the catalytic cycle turns over. This complete catalytic cycle is shown in Figure 4.11.

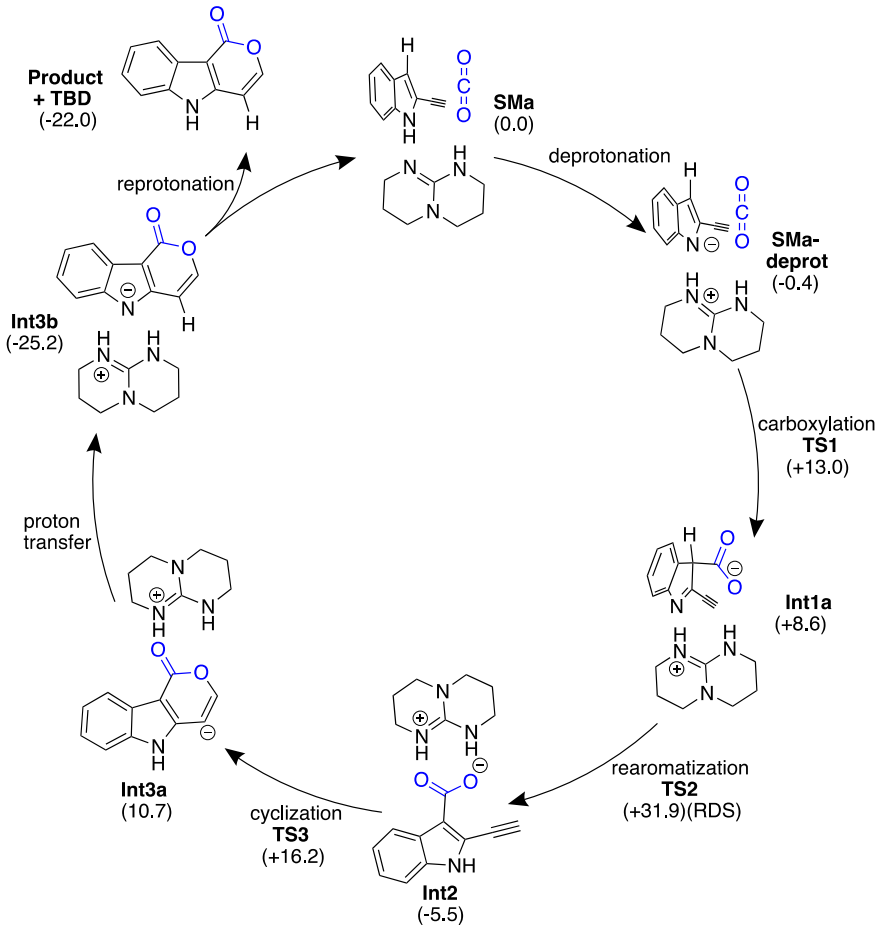

Figure 4.11. Computationally modelled catalytic cycle for the CO_2 trapping reaction from Skrydstrup *et al.* All Gibbs energies are shown in kcal/mol, relative to **SMa**. All structures shown were modelled with a methyl group bound to the ethyne moiety of the substrate, but this is omitted for clarity.

4.2 Rationalizing Kinetic Behaviour:

With a clear picture of the mechanism of this transformation now in mind, attention can be turned to the odd behaviour observed during the kinetic studies of this reaction. Kinetic studies of this reaction suggest a shift in catalyst rate order from one to zero as the reaction progresses past one catalyst turnover. Through this computational model, this can be rationalized by comparing the energies of the salts TBD forms with the starting substrate and the product. Relative to **SMa**, the formation of **SMa-deprot** is favourable by 0.4 kcal/mol. In comparison, the formation of **Int3b**

from free TBD and the neutral reaction product is favourable by 3.2 kcal/mol. This energy difference is visualized in Figure 4.12.

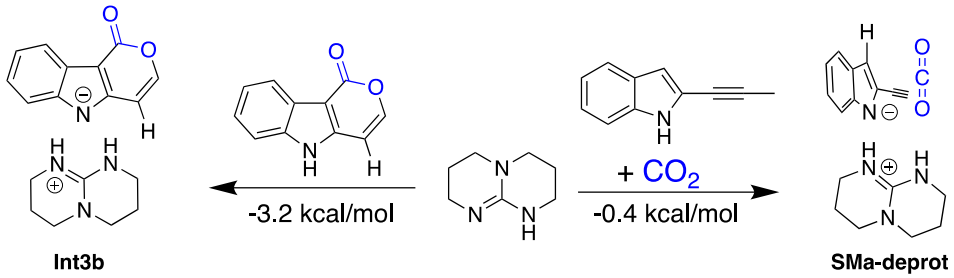

Figure 4.12. Reaction scheme comparing the energies of $TBDH^+$ salt formation between the starting substrate and the product of the reaction. Relative Gibbs energies are given in kcal/mol.

Because the mechanism of this reaction necessitates the initial formation of this ion pair with the substrate, the product of the reaction behaves as a catalyst deactivator. When the reaction has proceeded to the point of one catalyst turnover, there is an equimolar ratio of TBD and product. At this point the reaction becomes dissociation controlled, and the rate of the reaction is no longer dependent on the initial catalyst loading but on the equilibrium between the TBD:product salt and the two free neutral species. Additionally, as an experimental proof of this hypothesis, the different reaction rates between acetonitrile and diglyme are compared with the respective solvent properties. As stated previously, acetonitrile has a much higher dielectric constant than that of diglyme, which is one specific measure of solvent polarity. Practically, a solvent with a high dielectric constant is better able to insulate oppositely charged species from each other in solution. With this in mind, it follows that any step in this reaction which involves the production of charged species from neutral species would be more favourable in acetonitrile than in diglyme, as the resulting ion pairs are better stabilized by the solvent. Based on this, two assertions may be made. First, that the initial step of this reaction which involves the formation of **SMa-deprot** from **SMa** should be more favourable in acetonitrile than in diglyme. Second, that the last step of this reaction in which free TBD and product form from **Int3b** should be less favourable in acetonitrile than in

diglyme. Therefore, if this hypothesis concerning the changing rate behaviour is correct, it should be the case that this reaction proceeds faster in acetonitrile to the point of one catalyst turnover than it does in diglyme. At this point, the reaction rates should switch, and the dissociation-controlled process should be faster in diglyme than in acetonitrile. When the kinetic profiles of the reactions in acetonitrile and diglyme are compared, this rate switch is observed, as shown in Figure 4.13.

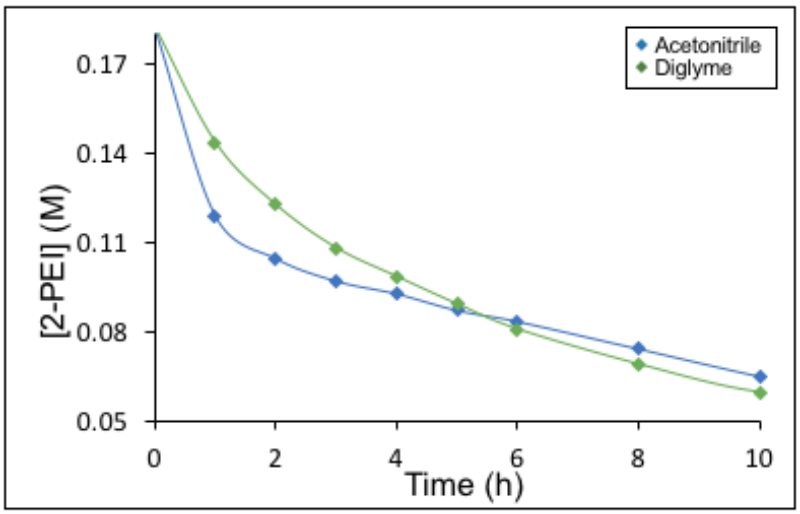

Figure 4.13. Kinetic profiles of the CO_2 trapping reaction in acetonitrile and diglyme compared. Both reactions compared are at 40 mol% TBD loading and otherwise identical conditions.

Although a mechanism for a chemical transformation can never be truly proven, this proposed catalytic cycle represents a significant improvement over the one postulated in the literature. This proposed pathway takes into consideration the significant experimental findings presented in the previous chapters, which allows for a more complete picture of the reaction to be inferred. The physical and mechanistic studies involving the TBD:CO_2 adduct demonstrated the need to develop a new model of reactivity in this system, which in tandem with the elucidation of the catalyst rate order from kinetic studies facilitated the development of the supramolecular assembly model in which TBD activates the system through coordinative catalysis. This model

provides a logical mechanism through which free CO_2 is sequestered at an elevated temperature, which would otherwise be entropically unfavourable. It also explains the multifunctionality of TBD observed during the mechanistic study of this reaction; with the roles of coordination catalyst, base, and proton shuttle all well demonstrated.

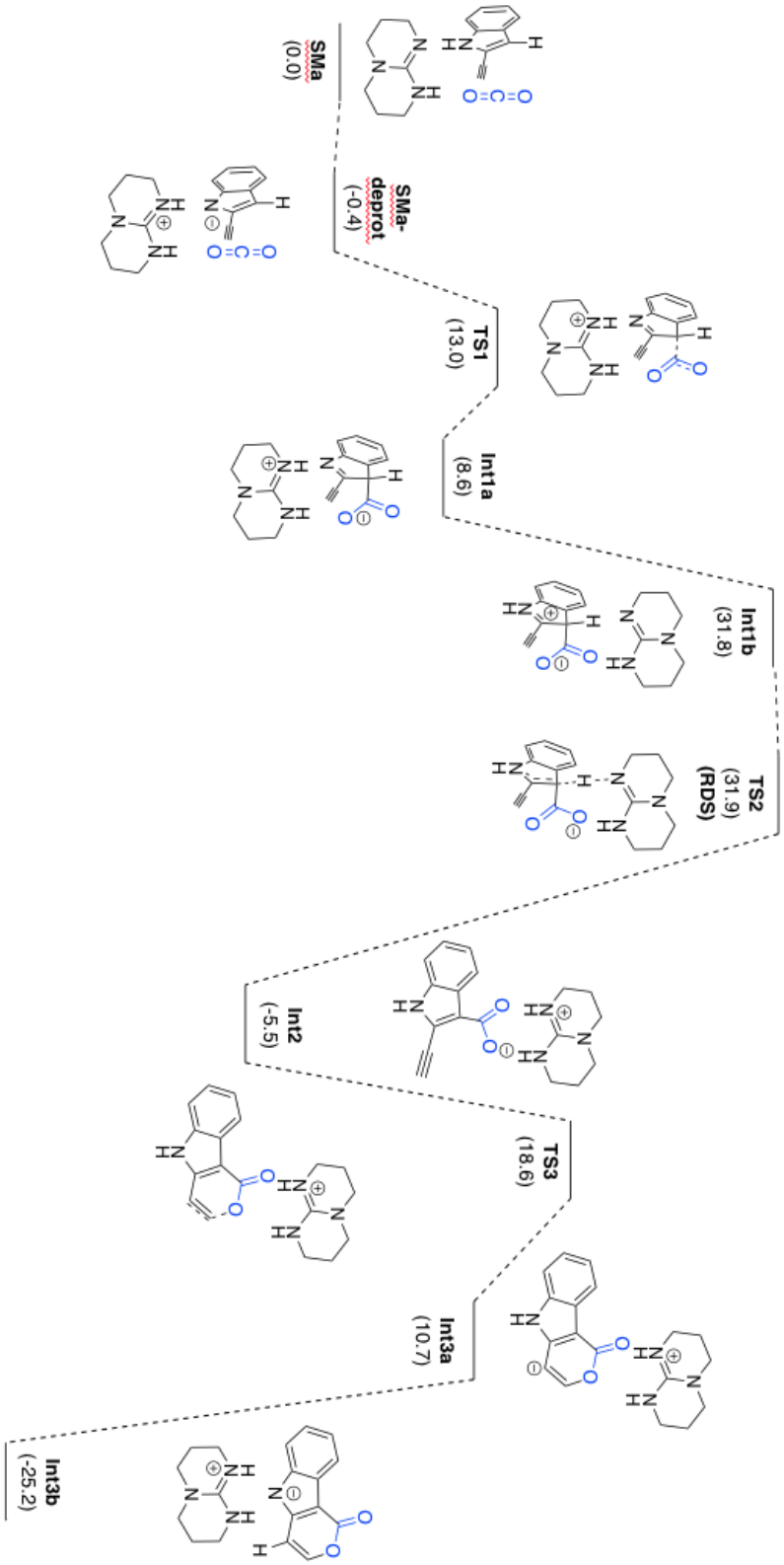

Figure 4.14. Complete energy diagram for the computational model of the CO_2 trapping reaction from Skrydstrup *et al.* All Gibbs energies are shown in kcal/mol, relative to **SMa**.

5. Novel CO_2 Trapping Substrate Design:

5.1. Introduction:

The final goal of this project was to apply what was learned and discovered about existing CO_2 sequestration reactions to the design of novel ones, in the hope of successfully creating a novel substrate or reaction capable of catalytic CO_2 sequestration. The number of existing sets of substrates and catalysts used in these processes is very limited, and they generally are all quite similar in terms of structure and mechanism, as is subsequently discussed. This field is obviously one which has great promise in terms of real-world application, and the design of novel reactions may prove to be a lucrative endeavour for those involved. For this reason, any individual or group with a thorough understanding of the current state of the field may have the ability to benefit both themselves and the environment in the continued pursuit of this field. To begin the process of developing new substrates and reactions to sequester CO_2, the essence of existing ones is subsequently discussed here.

5.2. Critical Analysis of Existing CO_2 Sequestration Reactions:

For CO_2 sequestration with non-commodity chemicals to truly represent the principles of green chemistry, and certainly to ever be economically viable, it must be achieved through catalytic processes. For this to be possible a candidate substrate must contain both a suitable nucleophile which can be carboxylated and a suitable electrophile which can accept the electron pair from the carboxylate anion. The end result of this process is a reaction that incorporates CO_2 into an otherwise unaltered molecular formula as shown in equation 1.

$$(1) \quad C_xH_aO_yN_b + CO_2 \rightarrow C_{x+1}H_aO_{y+2}N_b$$

Current substrates that fit this mold seem to rely exclusively on the incorporation of CO_2 in a heterocyclic ring structure as a lactone, usually by initial carboxylation followed by cyclization.[9,14,15]

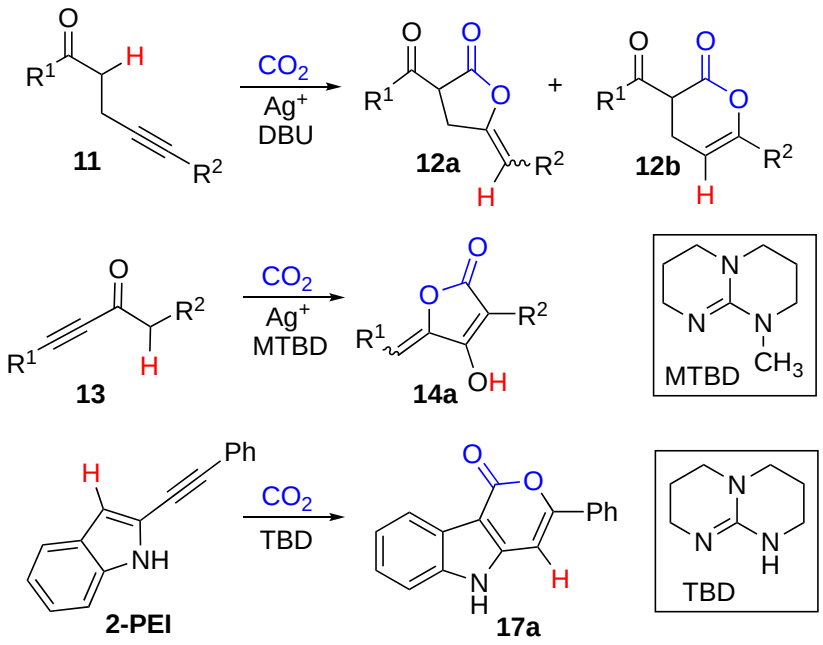

Figure 5.1. Products of CO_2 trapping reactions involving alkyne cyclizations with incorporated CO_2 molecule shown in blue and transferred proton in red.

In all of the processes shown in Figure 5.1, an alkyne is the electrophilic species. The nucleophilic species are enolates in **11** and **13**, and a trapped enamine in **2-PEI**. Exemplified in Figure 5.1, many C-C bond forming CO_2 trapping reactions rely on the use of silver(I) as a co-catalyst, or often as the only catalytic species with base in excess. In these reactions silver(I) ions are thought to activate the alkyne of the scaffold as an electrophile by accepting electron density from the alkyne, lowering the LUMO energy of the system. Upon intramolecular nucleophilic attack from the carboxylate ion, a silver-carbon sigma bond is formed temporarily, which abstracts a proton from the protonated base catalyst and regenerates both base and silver(I) catalyst as outlined in Figure 5.2.

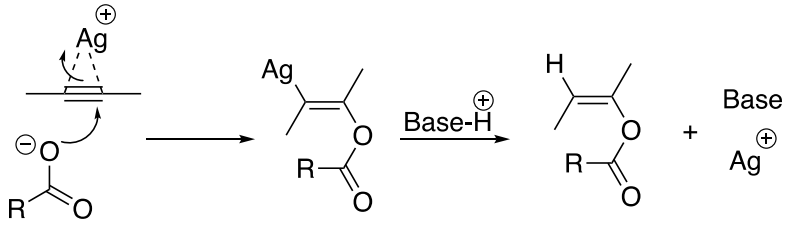

Figure 5.2. Mechanism of silver-catalyzed alkyne activation towards nucleophilic attack from carboxylate.

To understand this mechanism of alkyne activation, an analogy can be drawn to the Dewar-Chatt-Duncanson model of metal-alkene complexes, with the following examples illustrated in Figure 5.3. Silver(I), being in the highest oxidation state commonly encountered by silver, is not able to oxidatively add across the alkyne and form the silver(III) equivalent cyclopropene. Because of this, silver(I) acts only as a Lewis acid and accepts electron density from the alkyne and does not have electrons from its filled d-orbitals of appropriate symmetry back-donate significantly into the π^* antibonding orbitals of the alkyne. Thus, this activation mode is best described as forming a silver(I)-alkyne coordination complex, and not in a way reminiscent of a formal two-electron transfer to the alkyne, such as would be the case for a low-valent, electropositive early transition metal ion like titanium(II) as shown in Figure 5.3.

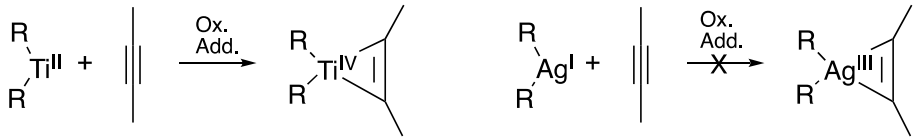

Figure 5.3. Different types of bonding in metal-alkyne complexes.

This distinction is important because various catalysts can activate alkynes as nucleophiles or electrophiles. In the context of these CO_2 sequestration processes, the electrophilic activation of the alkyne moieties is the necessary outcome. This requires a (co)-catalyst which will only accept electron density from, and not donate electron density to, the alkyne. However, as previously mentioned, there is no logical consistency between the literature substrate/catalyst

systems which do and do not need to be activated in this fashion. While an understanding of this method of alkyne activation catalysis is valuable, further work in developing this field should not treat this activation mode as absolutely necessary in all cases.

Similarly, in Figure 5.1 all three reactions shown have a carbon-based nucleophile in the substrate. All three substrates, while unlikely to be strong enough nucleophiles on their own, certainly need a base catalyst to allow the protons (shown in red) to be shuttled from starting material to product. A suitable base catalyst for these reactions must have the pKa of its conjugate acid (BH+) significantly high to allow for substrate deprotonation facilitating activation of carbon-centred nucleophiles, but also the capability to act catalytically by in turn transferring that proton to the formed carbanion. To meet these criteria the protonated base must remain in solution and be capable of establishing acid-base equilibrium with the substrate. Furthermore, these bases must be capable of being used at the elevated temperatures necessary for typical catalytic CO_2 sequestration reactions. This rules out conventional superbases such as sodium hydride or organolithium reagents, which react to completion with acidic substrates as their conjugate acids are evolved as gasses. Commonly employed bases are exemplified by the amidines and guanidines, which meet these criteria.

To determine appropriate substrates and base catalysts to use in CO_2 sequestration reactions, an understanding of their respective acidity and basicity is necessary. However, typical catalytic CO_2 sequestration reactions are incompatible with water for two reasons. First, water is acidic enough to protonate the typical guanidine and amidine bases used, which poisons their catalytic activity as demonstrated in Figure 5.4.[32] Second, water is a competent enough nucleophile to attack CO_2, and quickly establishes equilibria with bicarbonate, carbonate, and carbonic acid in solution. These species are also capable of reacting with base catalysts, forming salts which also

serve to poison the catalyst.[12] For these reasons, reactions of this type are conducted in polar aprotic solvents.

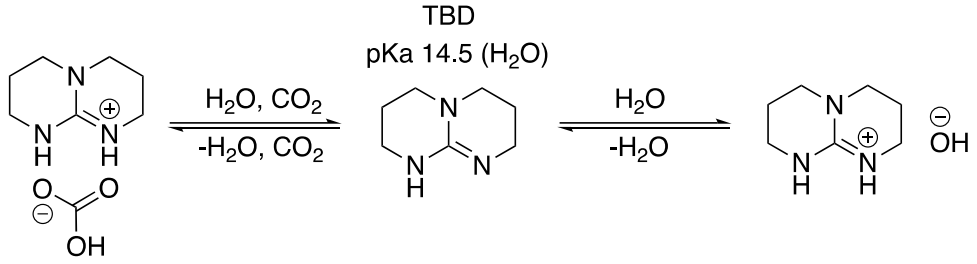

Figure 5.4. Scheme showing reactivity of TBD in aqueous media.

While typically associated with aqueous media, the concept of pKa can be applied to any solvent system. While nonsensical for solvents without any real ability to accept protons like cyclohexane, the concept is often applied to more Brönstead-basic solvents like acetonitrile, THF, and DMSO.[33] The experimental determination of acidity in acetonitrile is commonly done using spectroscopic methods, such as titration with UV-Vis spectroscopic analysis.[34] Sets of pKa data obtained by different methods and groups differ slightly but are experimentally determined in a way to keep them self-consistent. As in water, the pKa of an acid in any solvent is defined by the following set of equations:

$$(2) \quad HA + S \rightleftharpoons A^- + SH^+$$

$$(3) \quad K_a = \frac{[A^-][SH^+]}{[HA]}$$

$$(4) \quad pK_a = -log_{10}K_a$$

where HA and A^- represent an acid and its conjugate base, respectively, and S represents a solvent molecule. For example, in acetonitrile the pKa of an acid is calculated following equation 5:

$$(5) \quad H_3C{-}C{\equiv}N: + HA \underset{}{\overset{K_a}{\rightleftharpoons}} H_3C{-}C{\equiv}\overset{\oplus}{N}H + A^{\ominus}$$

The experimental pKa(MeCN) values of some of the common bases used in CO_2 sequestration reactions are shown in Table 5.1. The values shown actually represent the pKa of the conjugate acid of each base shown, however this is omitted throughout for clarity and consistency with literature.[35]With these values in mind, the designed CO_2 sequestration substrates must have an acidic proton with a pKa value roughly within three units of the base catalyst used.

Base:	pKa:[35]
MTBD	25.49
TBD	26.03
DBU	24.34
TMG	23.37

Table 5.1. Experimental pKa values of common organic amine superbases in acetonitrile.

In general, acidic C-H bonds arise from their proximity to electron-withdrawing groups such as carbonyl, nitro, or cyano groups. However, some C-H bonds are unusually acidic for other reasons such as those found in cyclopentadiene, for which the corresponding anion is stabilized through its resulting aromaticity. Another class of compounds to consider are those such as anilines, indoles, and phenols, which possess acidic protons on heteroatoms but tend to act as carbon-centred nucleophiles. All of these considerations were heeded in the envisioning of novel CO_2 sequestration reaction substrates.

5.3 Novel Substrate Design and Testing:

The distilled scaffold of most existing catalytic CO_2 sequestration substrates is shown in Figure 5.5. In this section, this model was used as a template for the design of new CO_2 sequestration substrate candidates.

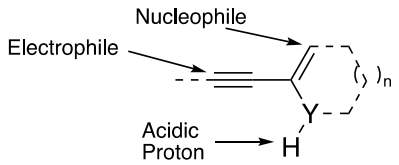

Figure 5.5. Chemical structure showing the skeleton of a CO_2 trapping substrate. Y indicates either a carbon atom or a protonated heteroatom. Dashed lines indicate substitution which may or may not be present.

As previously discussed, Figure 5.5 shows the three vital components to this scaffold which must be assembled synthetically. A few key points about this scaffold were considered during the substrate design for this project. The first difficulty associated with molecules of this class is their volatility. Small acetylenes and alkenes are generally quite volatile, which complicates substrate synthesis and experimental design. For this reason, the molecules were conceptually designed based on having a phenyl substituted alkyne as the electrophile in the scaffold. This consideration allows for using phenylacetylene (**28**) as a synthetic building block, which is an easily workable liquid. A selection of some of the scaffolds envisioned is shown in Figure 5.6.

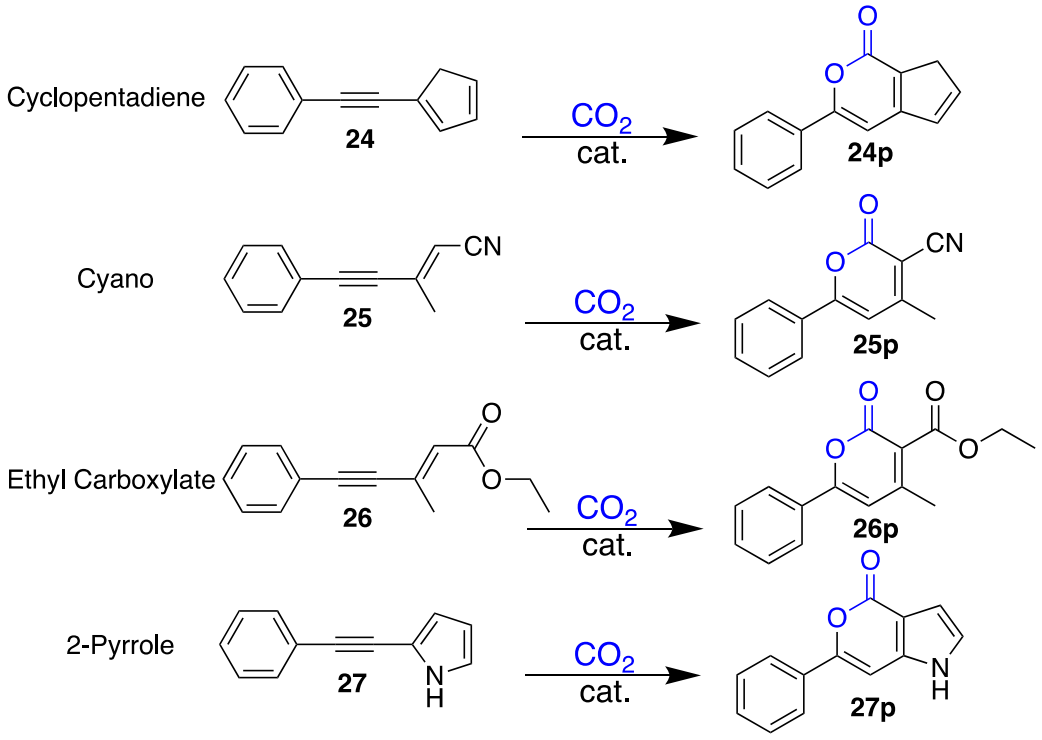

Figure 5.6. Representative sample of envisioned novel CO_2 trapping scaffolds showing the proposed pattern of CO_2 incorporation. Only the theoretical *6-endo-dig* cyclization products are shown here, but the *5-endo-dig* products could also be formed.

Of these compounds, a synthetic pathway towards **25** and **26** was chosen, as it was determined that both of these substrates could be produced from the ketone intermediate **29** shown in Figure 5.7.

This synthesis was indeed successful, and the cyano-substrate **25** was produced in a 69.3% yield over two steps.

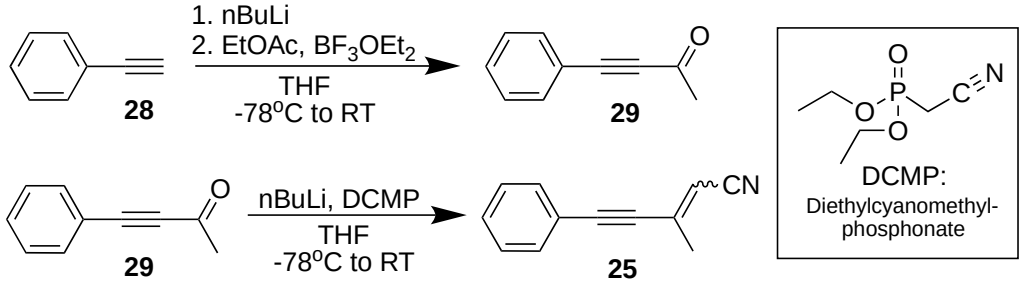

Figure 5.7. Reaction scheme depicting the synthesis of the cyano-substrate.

As there are no reported values for the pKa of **26** in the literature, and the cyano-substrate **25** has not previously been reported in the literature, an estimate of the pKa values is necessary. Table 5.2 shows the calculated pKa values for a few example substrates in water for reference, which are within the acceptable value range compared to TBD in this case. Unfortunately, the direct computational calculation of pKa values in acetonitrile is not as trivial.

Substance	**pKa(H_2O)**
Cyano-substrate (**25**)	16.76[a]
Ester-substrate (**26**)	15.60[a]
Nitro-substrate	8.18[a]
TBD	14.5[32]

Table 5.2. Theoretical pKa values of some novel CO_2 trapping substrates. [a]- See supplementary information for details concerning the calculation of these values.

As a more qualitative method of comparison, Figure 5.8 shows a comparison between **25** and a structurally similar unsaturated cyano compound.

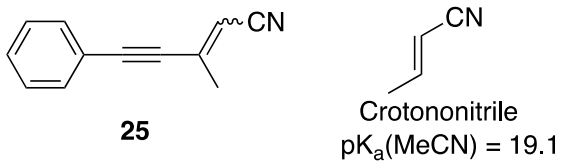

Figure 5.8. Structural comparison of cyano-substrate **25** and crotononitrile for purpose of pKa approximation.[36]

While this is a crude estimate, the pKa of crotononitrile in acetonitrile is ~5-7 orders of magnitude less than that of the bases commonly used in these sequestration reactions, so it is likely that the terminal methyl group of **25** can also be deprotonated by these bases. Indeed, preliminary testing found that TBD rapidly isomerized the alkene geometry in a single isomer of **25** in solution, which suggests that deprotonation of the terminal methyl group is indeed occurring. With this chosen substrate, a scope of conditions was then tested to attempt to create a novel catalytic CO_2 trapping reaction.

Of the conditions tested, an Au(I)/TBD system showed complete consumption of starting material over the time interval of the reaction. However, no attempts to isolate the formed product were successful, and both isomers of starting material **25** were obtained upon workup. With even the most delicate methods used, it appears whatever compounds are produced are too unstable to be isolated with the methods used. Upon retrospective analysis of the theoretical product of this reaction, the addition of an electron-withdrawing carboxylate group to the already polarized cyano-alkene may make this particular compound simply too prone to hydrolysis. Future work on these systems should be focused on systems in which this alkene is stabilized by being in an aromatic ring to mitigate this issue. Unfortunately, the experimental study of this system was concluded at this time due to unforeseen circumstances.

6. Conclusions and Going Forwards:

The work presented in this thesis has given the reader a solid foothold on the current state of carbon dioxide activation and sequestration chemistry. Through a combination of the overview of relevant catalytic CO_2 sequestration reactions presented in section 1 with the experimental and theoretical work of sections 2-4, this work provides a vantage point from which future discussion and development of the field can be viewed. Specific aspects of the work presented in the preceding sections have not previously been reported, including the first demonstration of changing-order catalysis in a CO_2 sequestration reaction and the mechanistic work involving the TBD:CO_2 adduct which was previously invoked as an on-cycle species in these processes. Following these experimental results, this work demonstrated the process for constructing an informed theoretical model of the CO_2 sequestration reaction which was studied. The final section of this work then demonstrates the informed proposal of new CO_2 sequestration substrates, with consideration of all the information presented before it.

As work in this field progresses, there will be an increased focus on the development of carbon-carbon bond forming reactions. In addition, the conceptual limit of only alkynes as suitable electrophiles must also be expanded, with continued development investigating the more challenging and yet unreported use of electrophilic alkene-containing substrates as well. While the current understanding of how transition metal catalysis effects these transformations remains unclear, research must not initially focus on the development of metal-free processes, as this will limit the realization of the full scope of possible reactions. Through further development and mechanistic study of these processes, the precise mechanism of transition metal-catalyzed activation will eventually be revealed. This in turn will guide the development of metal-free reactions which can mimic the mechanisms of transition metal-catalyzed reactivity.

7. References:

1. Kolbe, H. *Justus Liebigs Annalen der Chemie.* **1860**
2. Urea. *Ullmann's Encyclopedia of Industrial Chemistry,* 5th ed.; VCH: Weinheim, Germany, 2010; pp 657-693.
3. Carbonic Esters. *Ullmann's Encyclopedia of Industrial Chemistry,* 5th ed.; VCH: Weinheim, Germany, 2012; pp 45-62.
4. Shaik, A.A.G., Sivaram, S. *Chem. Rev.* **1996**. 96, 951-976.
5. Grignard, V. *Compt. Rend.* **1900,** 130, 1322.
6. Flowers, B., Gantreau-Service, R., Jessop, P. *Adv. Synth. Cat.* **2008**, *350*, 2947-2958.
7. Fan, Y. *et al. J. Org. Chem.* **2018,** 83, 17, 9991-10000.
8. Zhou, H., Zhang, R., Lu, X. *Adv. Synth. Cat.* **2019,** 361, 2, 326-334.
9. Xin, Z., Lescot, C., Friis, S. D., Daasbjerg, K., Skrydstrup, T. *Angew Chem.* **2015,** *127*, 6966-6970.
10. Yoshida, M., Mizuguchi, T., Shishido, K. *Chem. Eur. J.* **2012,** 18, 15578-15581.
11. Lu, X., *et al. J. Org. Chem.* **2008,** *73,* 8039-8044.
12. Nichols,R., Kaufhold., Nguyen, B.N. *Catal. Sci. Technol.* **2014,** 4, 3458-3462.
13. Ca, N. D., Gabriele, B., Ruffolo, G., Veltri, L., Zanettaand, T., Costa, M. *Adv. Synth. Catal*. **2011**, 353, 133–146.
14. Kikuchi, S., Sekine, K., Ishida, T., Yamada, T. *Angew. Chem. Int. Ed.* **2012,** 51, 28, 6989-6992.
15. Sadamitsu, K., Komatsuki, K., Saito, K., Yamada, T. *Org. Lett.* **2017,** 19, 3191-3194.
16. Takahashi, I., Ojima, N., Ogura, K., Seto, S. *Biochemistry* **1978,** 17, 13, 2696–2702.
17. Yoo, W., Capdevilla, M. G., Du, X., Kobayashi, S. *Org. Lett.* **2012,** 14, 20, 5326-5329.

18. Praveen, C., Ananth, D. *Bioorg. Med. Chem. Lett.* **2016,** 26, 2507-2512.

19. Franco, D. W., *et al. J. Org. Chem.* **2004,** *69, 8005-8011.*

20. *CRC Handbook of Chemistry and Physics*, 85th ed.; Boca Raton, FL, 2004.

21. Becke, A. D. *J. Chem. Phys.* **1993,** 98, 5648-5652.

22. Lee, C., Yang, W., Parr, R. G. *Phys. Rev. B.* **1988,** 37, 785-789.

23. Ditchfield, R., Hehre, W. J., Pople, J. A. *J. Chem. Phys.* **1971,** 54, 724-728.

24. Hehre, W. J., Ditchfield, R., Pople, J. A. *J. Chem. Phys.* **1972,** 56, 2257-2261.

25. Zhao, Y., Truhlar, D. G. *Theor. Chem. Acc.* **2007,** 120, 215-241.

26. Krishnan, R., Binkley, J. S., Seeger, R., Pople, J. A. *J. Chem. Phys.* **1980,** 72, 650-654.

27. Frisch, M. J. *et al. Gaussian 09W Reference,* Gaussian, INC., Wallingford, CT, 2009.

28. Frisch, M. J. *et al. GaussView 5 Reference,* Gaussian, INC., Wallingford, CT, 2009.

29. Plumley, J. A., Dannenberg, J. J. *J. Comput. Chem.* **2011,** 32, 8, 1519-1527.

30. Steiner, T. *Angew. Chem. Int. Ed.* **2002,** 41, 48-76.

31. Guthrie, J. P. *J. Am. Chem. Soc.* **1996,** 118, 12886-12890.

32. Yu, K. M. K., Curcic, I., Gabriel, J., Morganstewart, H., Tsang, S. C. *J. Phys. Chem. A* **2010,** *114,* 3863-3872.

33. Leito, I. *et al. Eur. J. Org. Chem.* **2019,** *40,* 6735-6748.

34. Koppel, I. A. *et al. J. Org. Chem.* **2006,** *71,* 2829-2838.

35. Kaupmees, A., Trummal, A., Leito, I. *Croat. Chem. Acta.* **2014,** *87,* 385-395.

36. Deniau, G., Thome, T., Gaudin, D., Bureau, C., Lecayon, G. *J. Electroanal. Chem.* **1998,** *451,* 145-161.

8. Supplementary Information:

Procedure for the synthesis of o-nitro-gem-dibromovinylbenzene.[1]

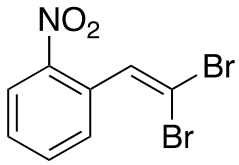

To a solution of ortho-nitrobenzaldehyde (1.51 g, 10mmol) and carbon tetrabromide (4.98 g, 15mmol) in 50 mL DCM is slowly added a solution of triphenylphosphine (7.87 g, 30 mmol) in 40 mL DCM at 0 °C. The mixture is allowed to stir at 0 °C for 30 minutes and then at room temperature for 60 minutes. The mixture is filtered through a silica plug which is washed with a small portion of DCM and then concentrated *in vacuo*. The crude residue of this reaction is used without further purification.

Procedure for the synthesis of o-gem-dibromovinylaniline.[1]

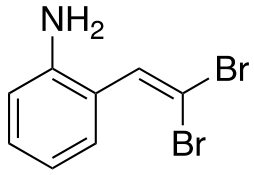

The crude residue from the synthesis of o-nitro-gem-dibromovinylbenzene is dissolved in a solution of 21 mL anhydrous ethanol and 3.5 mL glacial acetic acid. To the solution is added iron powder (4.0 g, 70 mmol) and iron (III) chloride (0.25 g, 1.5 mmol), and the mixture is refluxed. The progress of the reaction is monitored by TLC (7:1 hexanes:EtOAc). Upon complete conversion of starting material the reaction is filtered through a silica plug which is washed with a small amount of methanol and concentrated *in vacuo*. The crude residue is purified by flash column chromatography (7:1 hexanes:EtOAc) to give the product aniline (1.76 g, 6.35 mmol) as a brown oil in a 63.5% yield over two steps. The ^{1}H and ^{13}C NMR spectra are consistent with those reported in the literature.

^{1}H NMR (300 MHz, $CDCl_3$): δ=3.70 (br s, 2H), 6.69-6.74 (d, 1H), 6.76-6.83 (t, 1H), 7.13-7.20 (t, 1H), 7.28-7.33 (d, 1H) 7.34 (s, 1H).

Procedure for the synthesis of 2-phenylethynylindole.[1]

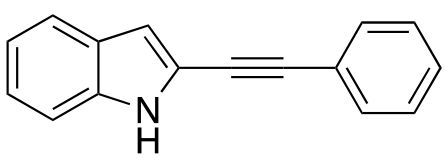

To a 100 mL round-bottom flask is added 10% w/w Pd/C (0.358 g, 0.32 mmol), triphenylphosphine (0.2g, 0.76 mmol), and a stir bar. The flask is equipped with a septum and is purged with argon for 10 minutes. To a second 100 mL pear-shaped flask is added o-gem-dibromovinylaniline (1.76 g, 6.36 mmol) and copper (I) iodide (35 mg, 0.18 mmol), and a stir bar. The flask is equipped with a septum and purged with argon for 10 minutes. After purging, a solution of phenylacetylene (1.04 mL, 9.4 mmol) and diisopropylamine (2.21 mL, 15.6 mmol) in 60 mL dry toluene is added to the flask containing vinylaniline and cuprous iodide via syringe. This mixture is stirred until homogeneity is obtained, and then cannulated to the first flask containing Pd/C and triphenylphosphine. The resulting mixture is heated at 100 °C for 2 hours. The mixture is then diluted with 100 mL Et_2O, filtered, washed with 70 mL H_2O and 50 mL brine, and dried with anhydrous $MgSO_4$. The solvent is concentrated *in vacuo* an the crude residue is purified by flash column chromatography with gradient elution (19:1 to 9:1 hexanes:EtOAc) affording the product 2-phenylethynylindole (0.963g, 4.44 mmol) as a pale-yellow solid in a 67.0% yield. The ^{1}H and ^{13}C NMR spectra are consistent with those reported in the literature. ^{1}H NMR (300 MHz, $CDCl_3$): δ=6.89 (s, 1H), 7.15-7.22 (t, 1H), 7.26-7.32 (t, 1H), 7.36-7.45 (m, 4H) 7.56-7.62 (m, 2H), 7.63-7.68 (d, 1H) 8.28 (br s, 1H).

Procedure for the synthesis of 1-methyl-2-phenylethynylindole.

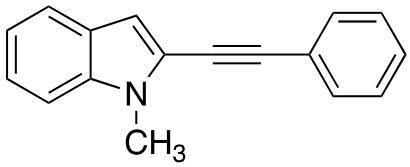

To a solution of 2-phenylethynylindole (14.5 mg, 0.067 mmol) in 1 mL dry DMF is added 60% w/w NaH in oil (6.0 mg, 0.15 mmol) with stirring. The solution rapidly turns from a straw-yellow colour to a deep red. Upon cessation of gas evolution, methyl iodide (5 μL, 0.080 mmol) is added and the mixture is stirred for 2 hours. The mixture is diluted with 10 mL Et_2O, washed with three portions of sat. $LiCl_{(aq)}$ solution and dried over anhydrous $MgSO_4$. The solvent in concentrated *in vacuo* and the crude product is purified by flash column chromatography (9:1 v/v hexanes:EtOAc) affording the product 1-methyl-2-phenylethynylindole (13.8 mg, 0.0597 mmol) as a pale-yellow solid in an 89.5% yield. The ^{1}H and ^{13}C NMR spectra are consistent with those reported in the literature.[2] ^{1}H NMR (300 MHz, $CDCl_3$): δ=3.92 (s, 3H), 6.88 (s, 1H), 7.28-7.35 (m, 2H), 7.39-7.45 (m, 3H), 7.59-7.67 (m, 3H).

Procedure for the synthesis of TBD:CO_2 adduct.[3]

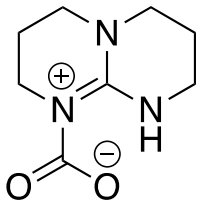

To a thick-walled screw-capped test tube is added a solution of TBD (60.5 mg, 0.43 mmol) in 0.5 mL dry THF. The mixture is cooled to -196 °C, degassed under vacuum, and back-filled with CO_2. Upon warming to room temperature, the product TBD:CO_2 adduct is obtained as a milky-white suspension in quantitative yield. The crude residue of this reaction is used without further purification.

Procedure for the synthesis of 4-phenylbut-3-yn-2-one.[4]

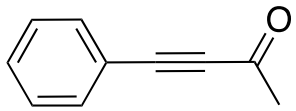

To a solution of phenylacetylene (0.440 mL, 4 mmol) in 6 mL dry, degassed THF is added dropwise a solution of n-BuLi in hexanes (2.5 M, 1.8 mL, 4.5 mmol) at -78 °C. After stirring for 30 minutes, a solution of ethyl acetate (0.4 mL, 4.1 mmol) in 6 mL dry, degassed THF and neat BF_3OEt_2 (0.76 mL, 6 mmol) are added sequentially at -78 °C. The mixture is stirred for an additional 30 minuted at -78 °C, and then for 1 hour at 0 °C. The reaction is quenched by the addition of 4 mL sat. $NH_4Cl_{(aq)}$, and diluted with 10 mL H_2O. The mixture is extracted with EtOAc (3x10mL), and the pooled organic layers are washed with water (3x10 mL), brine (2x5 mL), and dried with anhydrous $MgSO_4$. The crude mixture is concentrated *in vacuo* and purified by flash column chromatography (9:1 v/v hexanes:EtOAc) affording the product 4-phenylbut-3-yn-2-one (396 mg, 2.75 mmol) as a colourless oil in a 68.7% yield. The ^1H and ^{13}C NMR spectra are consistent with those reported in the literature. ^1H NMR (300 MHz, $CDCl_3$): δ=2.50 (s, 3H), 7.38-7.49 (m, 3H), 7.59-7.64 (d, 2H).

Procedure for the synthesis of 3-methyl-5-phenyl-2-penten-4-ynenitrile.

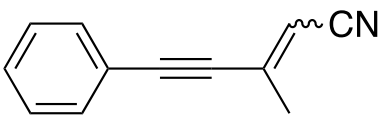

To a suspension of potassium tert-butoxide (275 mg, 2.44 mmol) in 3 mL dry, degassed THF is slowly added a solution of diethyl cyanomethylphosphonate (0.359 mL, 2.22 mmol) in 3 mL dry, degassed THF while stirring at 0 °C. The mixture is left to stir at 0 °C for 20 minutes, at which point the suspension clears to a pale yellow solution. A solution of 4-phenylbut-3-yn-2-one (320 mg, 2.22 mmol) in 4 mL dry, degassed THF is then added dropwise over 15 minutes with rapid stirring while at 0 °C. The mixture becomes a deep red colour and thickens slightly, is left to warm to room temperature, and is stirred for an additional 90 minutes. The mixture is then diluted with 50 mL EtOAc and washed with 50 mL H_2O. The aqueous layer is saturated with NH_4Cl and extracted with EtOAc (3x5 mL). The pooled organic layers are washed with sat. $NaHCO_{3(aq)}$ and brine (2x10 mL) and dried with anhydrous $MgSO_4$. The crude mixture is concentrated *in vacuo* and purified by flash column chromatography (9:1 v/v hexanes:EtOAc), affording the product 3-methyl-5-phenyl-2-penten-4-ynenitrile (257 mg, 1.54 mmol) as a mixture of isomers (55:45 E:Z) in a 69.3% yield.

Material Data for 3-methyl-5-phenyl-trans-2-penten-4-ynenitrile.[5]

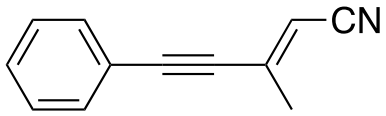

Pale yellow-green oil; m.p. 5-7 °C; ^{1}H NMR (300 MHz, $CDCl_3$): δ=2.30 (s, 3H), 5.65 (s, 1H), 7.30-7.45 (m, 3H), 7.50-7.59 (m, 2H); ^{13}C NMR (75 MHz, $CDCl_3$): δ=23.5, 86.5, 99.8, 103.1, 117.2, 121.9, 128.8, 129.4, 132.2, 142.5.

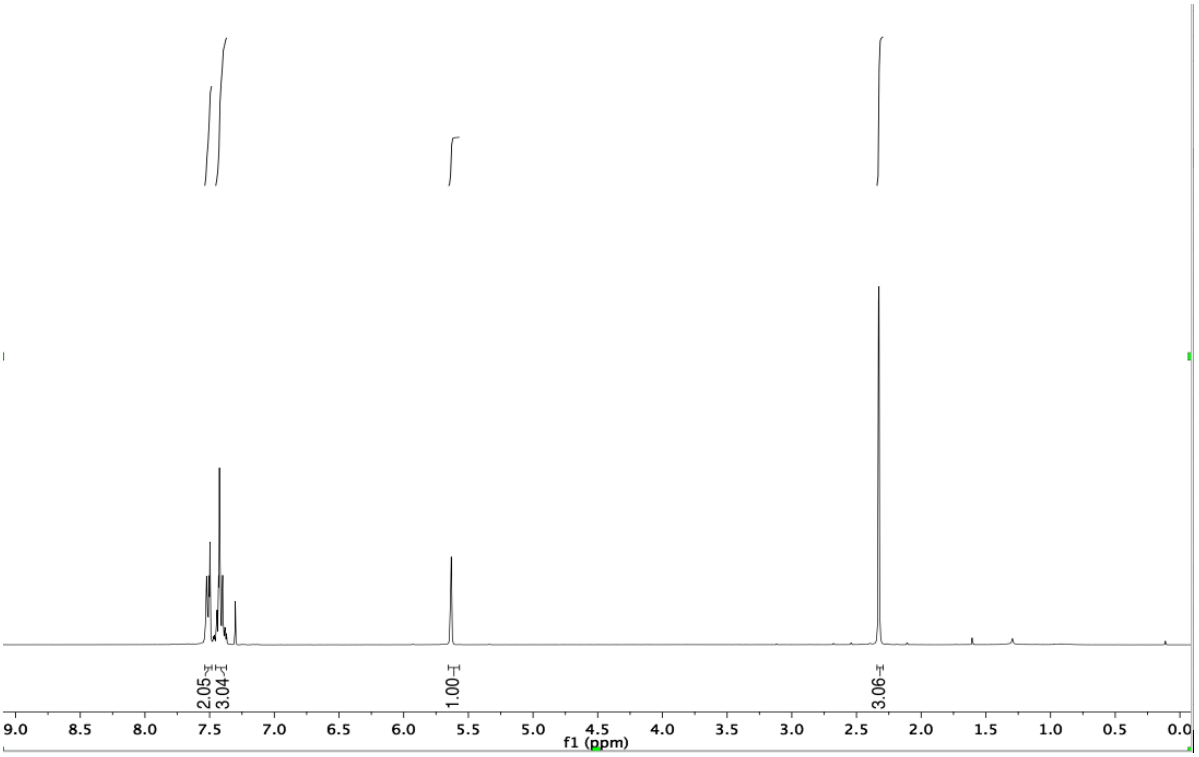

Figure S1. ^{1}H NMR (300 MHz, $CDCl_3$) spectrum of 3-methyl-5-phenyl-trans-2-penten-4-ynenitrile.

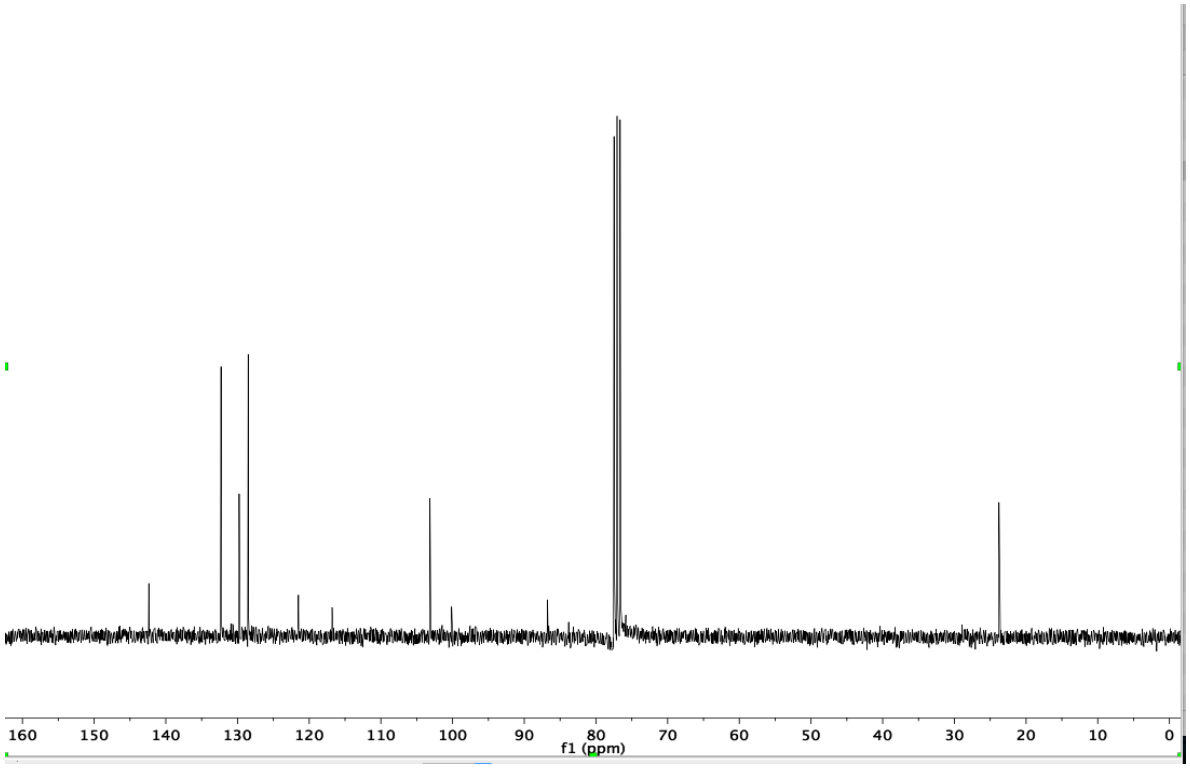

Figure S2. ^{13}C NMR (75 MHz, $CDCl_3$) spectrum of 3-methyl-5-phenyl-trans-2-penten-4-ynenitrile.

Procedure for the calculation of theoretical CO_2 trapping substrate pKas.

Molecular geometries were optimized for each compound using TURBOmole[6], with the BP86 functional[7,8] and the def2-TZVPD basis set[9,10] for each element. COSMOtherm was then utilized to calculate the pKa values of the compounds in water at 25 ^{o}C.

Optimized geometries and coordinates of intermediates and transition states calculated in Chapter 4.

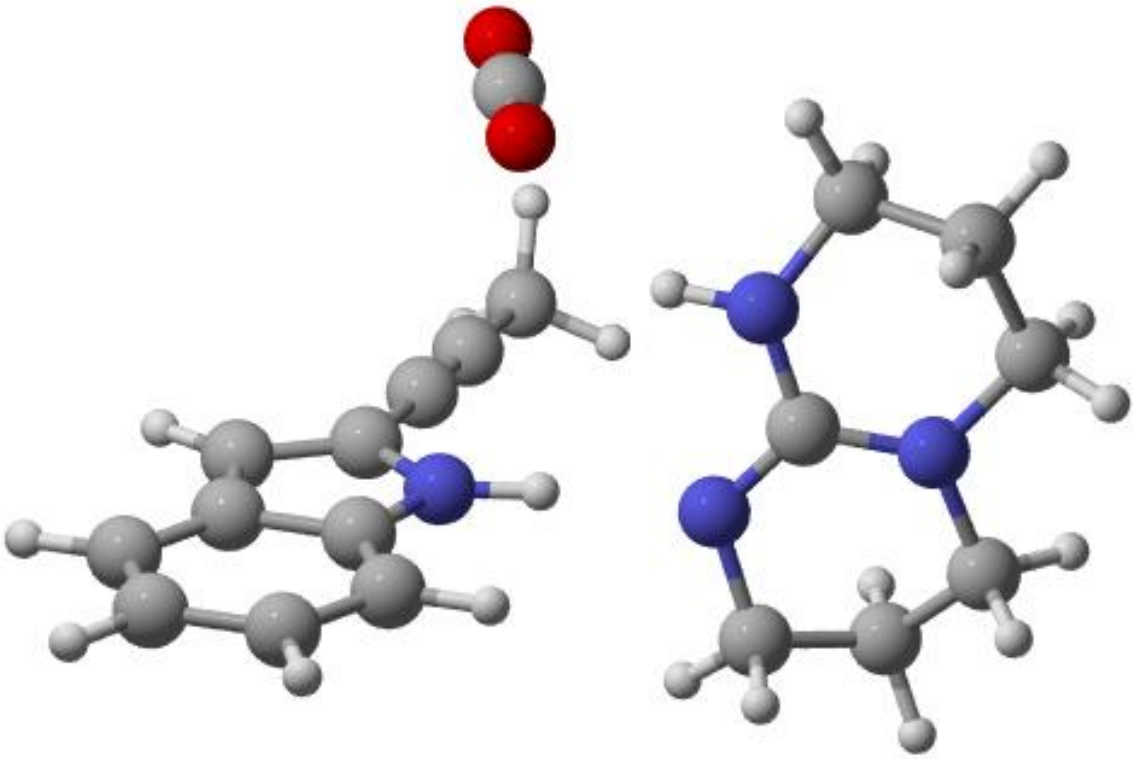

Figure S1. Optimized geometry of **SMa**.

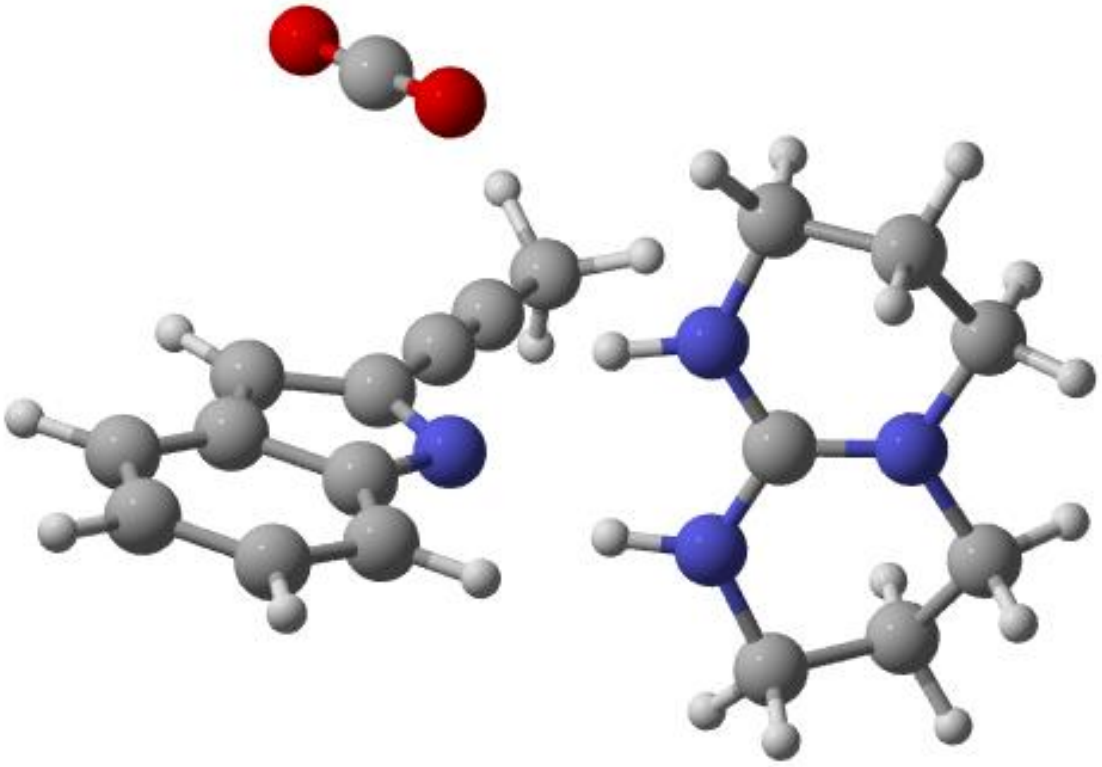

Figure S2. Optimized geometry of **SMa-deprot**.

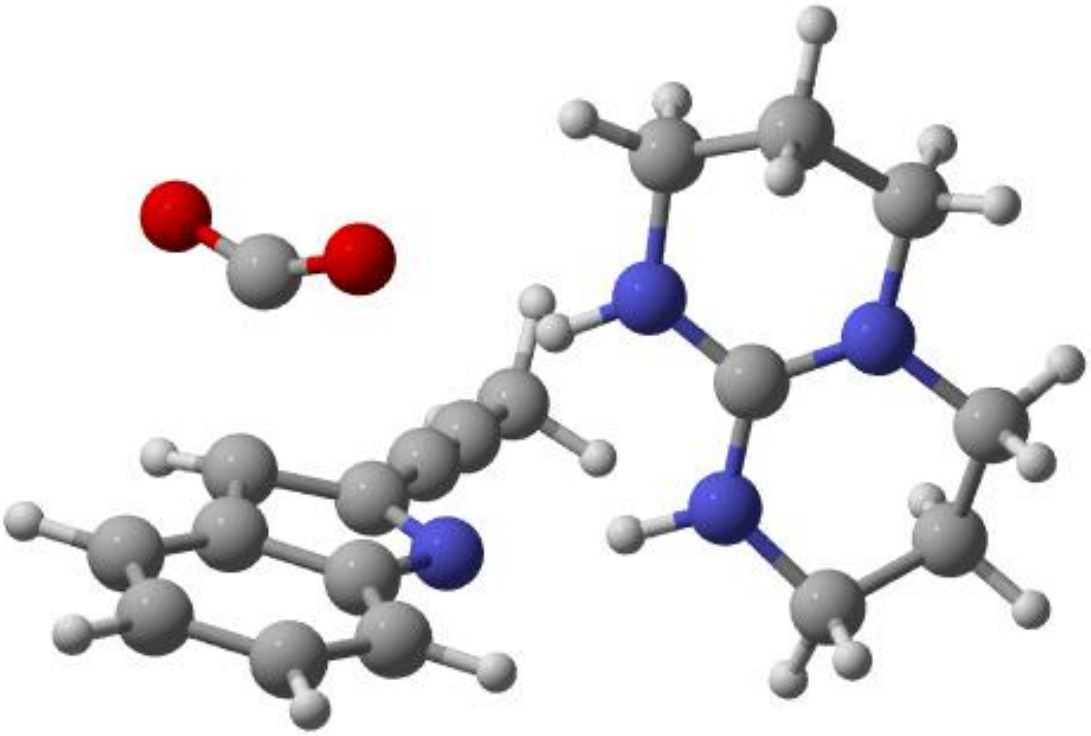

Figure S3. Optimized geometry of **TS1**.

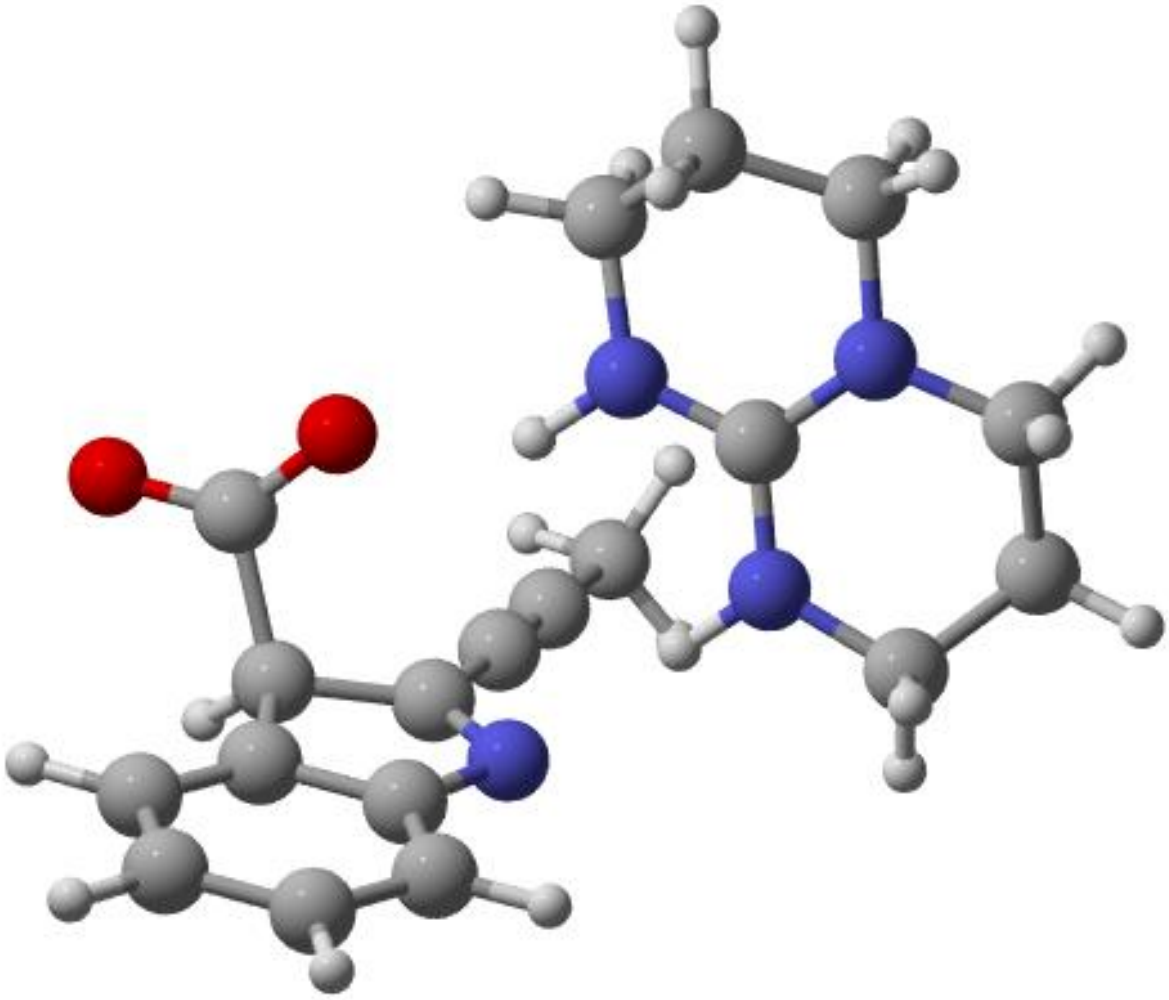

Figure S4. Optimized geometry of **Int1a**.

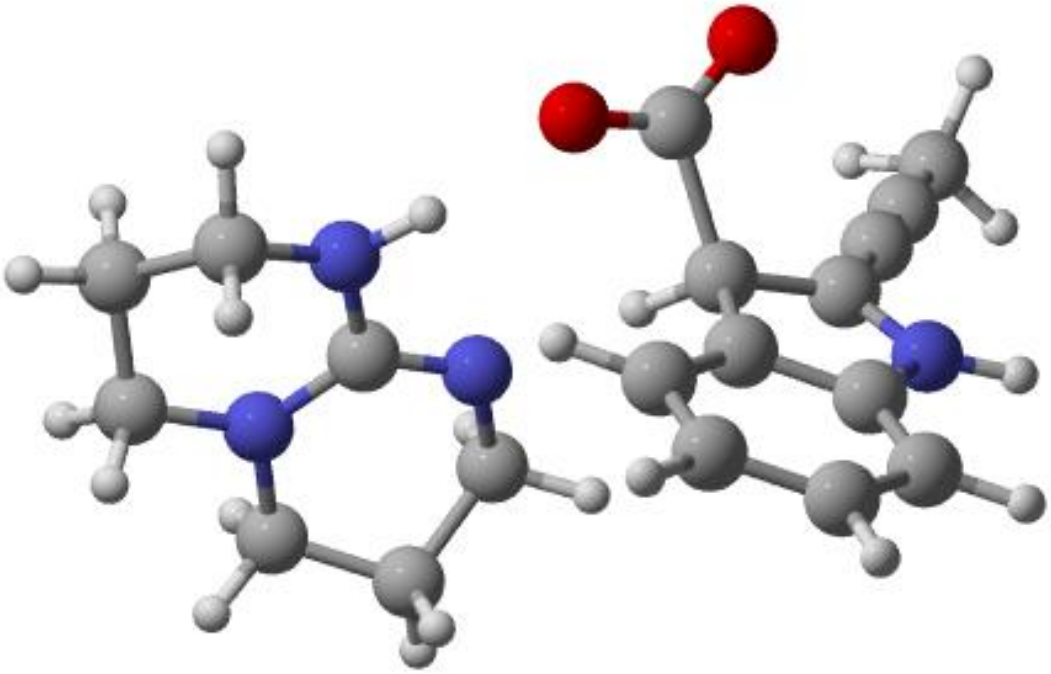

Figure S5. Optimized geometry of **Int1b**.

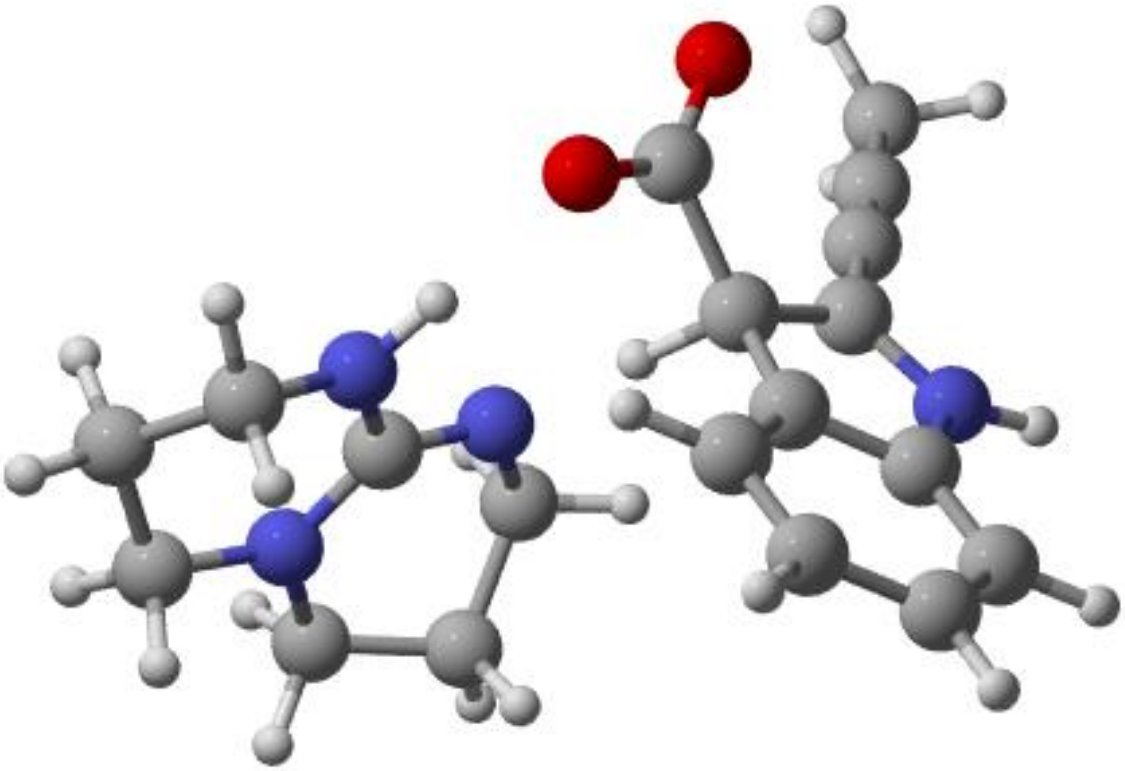

Figure S6. Optimized geometry of **TS2**.

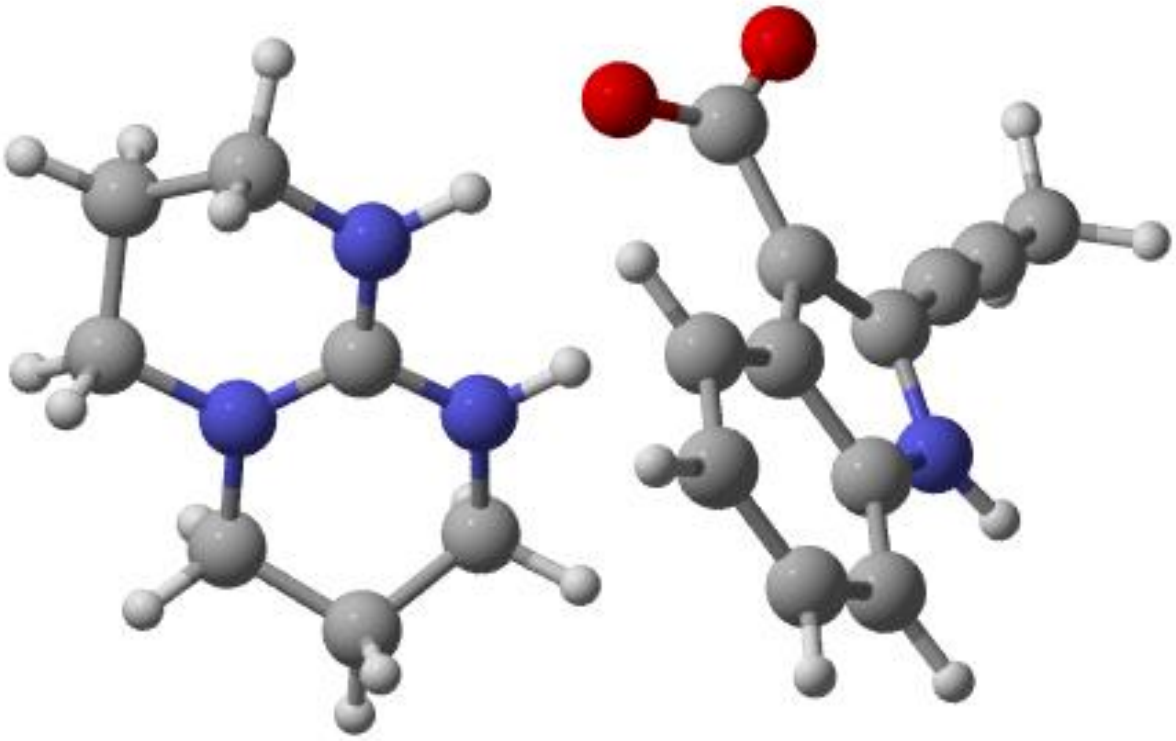

Figure S7. Optimized geometry of **Int2**.

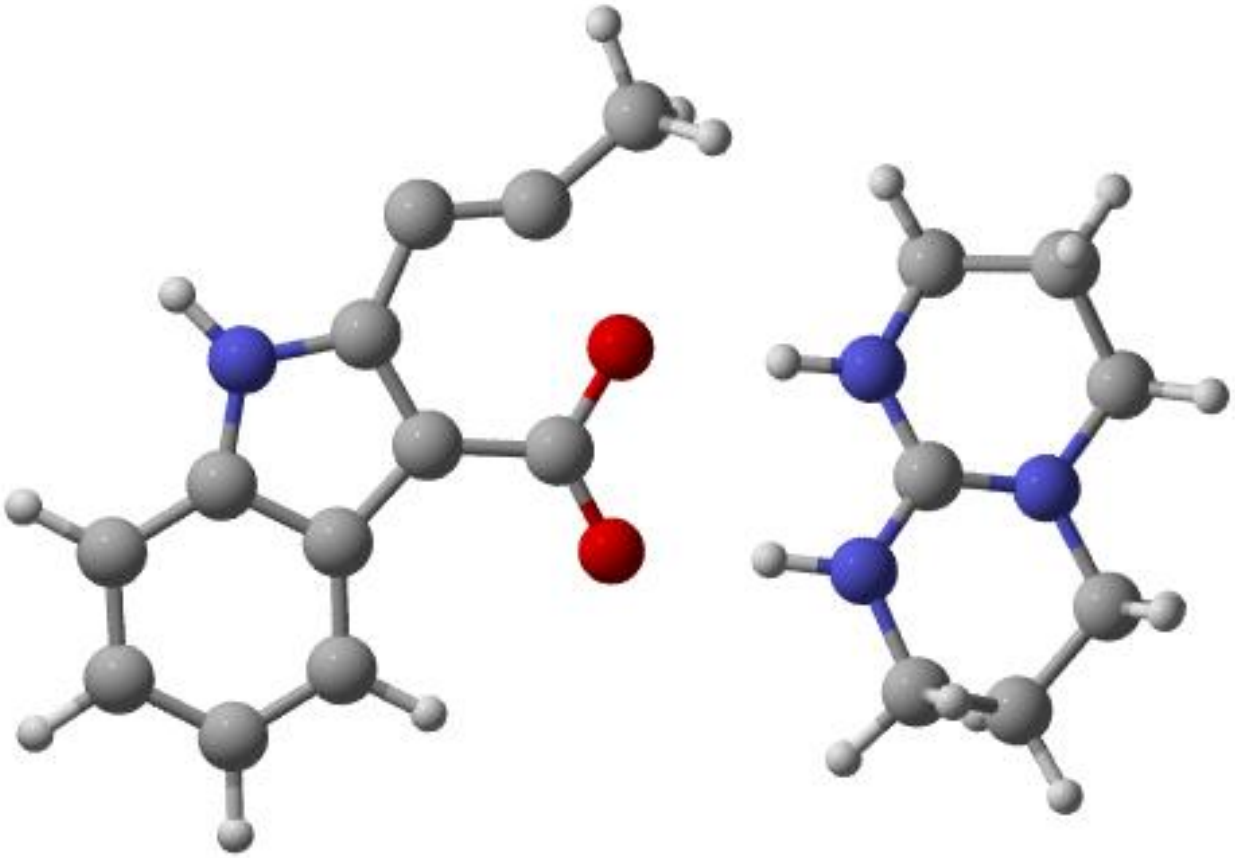

Figure S8. Optimized geometry of **TS3**.

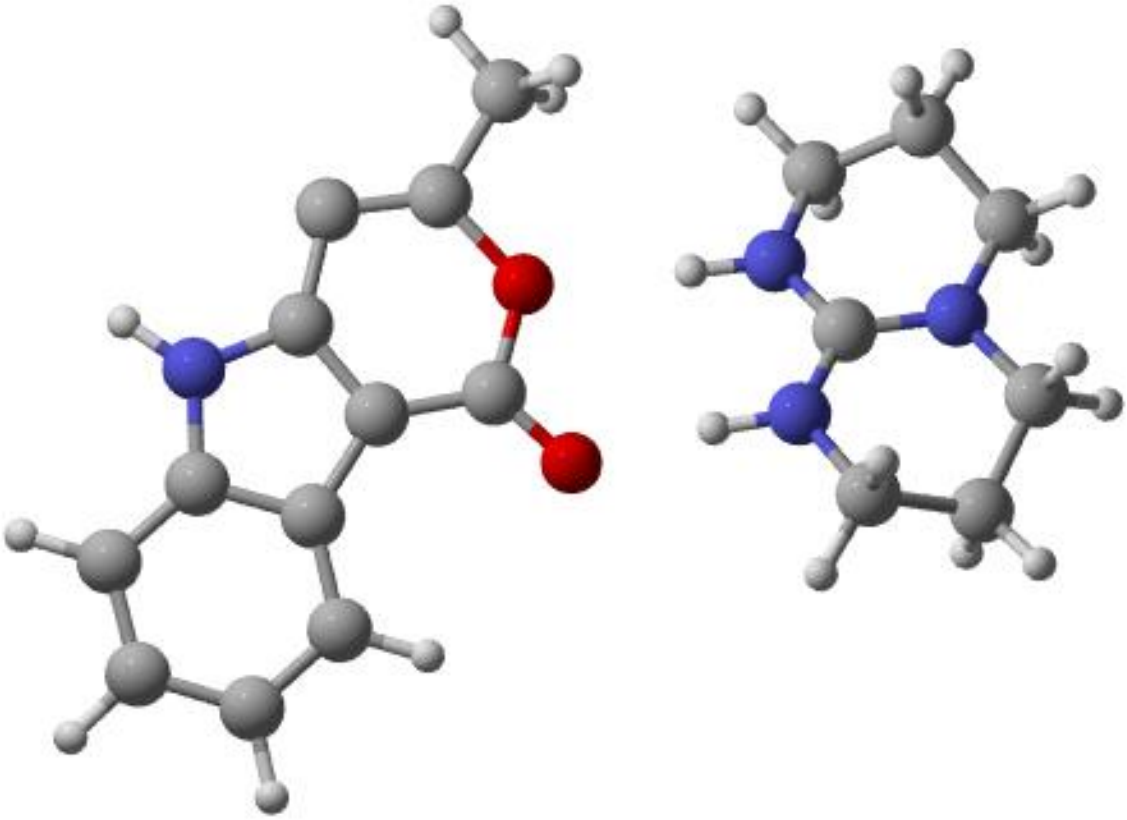

Figure S9. Optimized geometry of **Int3a**.

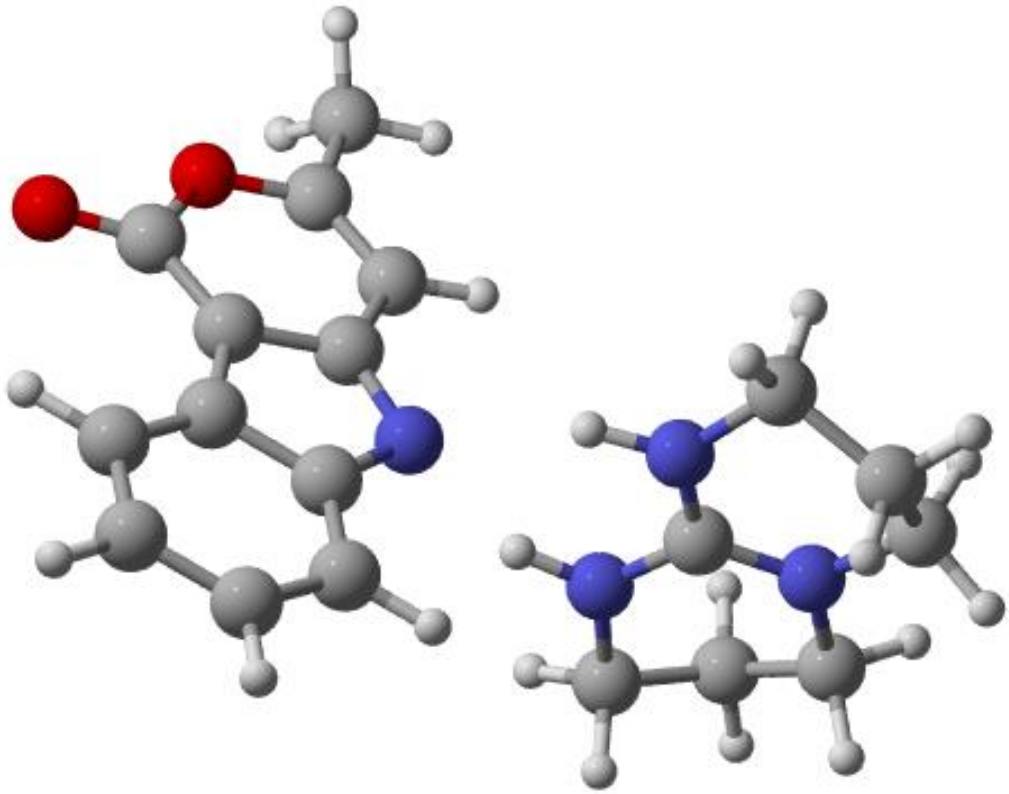

Figure S10. Optimized geometry of **Int3b**.

Atomic Coordinates of **SMa**:

C	-3.84266	-0.49906	-0.00199
C	-2.57726	-1.16135	0.05858
C	-2.45068	-2.47715	0.52892
C	-3.60673	-3.13014	0.93929
C	-4.86819	-2.49286	0.88709
C	-4.99557	-1.19035	0.42309
C	-3.59367	0.80655	-0.52475
C	-2.22902	0.89813	-0.76027
H	-1.48062	-2.9646	0.56895
H	-3.54064	-4.15038	1.30806
H	-5.75047	-3.0354	1.21674
H	-5.96992	-0.70892	0.38695
H	-4.31537	1.59038	-0.71074
N	-1.61797	-0.29626	-0.40442
C	-1.48406	1.98673	-1.28186
C	-0.863	2.926	-1.73798
C	-0.12059	4.05227	-2.29749
H	0.79305	3.71156	-2.79865
H	-0.72357	4.59394	-3.03585
H	0.17128	4.76357	-1.51592
C	-0.09204	3.33007	1.60125
O	-0.04049	4.44491	1.25713
O	-0.13924	2.21891	1.96427
C	2.15779	-0.81449	0.06219
N	1.92462	-0.16854	1.26358
H	1.04231	0.32742	1.27281
N	1.1364	-1.00291	-0.73001
N	3.43878	-1.25274	-0.17106
C	3.00882	0.42723	2.03356
C	4.57329	-0.98631	0.71969
C	4.12967	-0.6013	2.1274
C	3.78685	-1.87698	-1.45169
C	1.35485	-1.76859	-1.9518
C	2.75484	-1.54672	-2.52527
H	0.59098	-1.47485	-2.6821
H	1.20566	-2.84586	-1.76611
H	2.86062	-0.49779	-2.82887
H	2.92949	-2.16989	-3.40904
H	4.77777	-1.50998	-1.74613
H	3.87272	-2.96572	-1.31968
H	5.19717	-1.88825	0.7505
H	5.19183	-0.18431	0.28724
H	4.98464	-0.19851	2.67939
H	3.76339	-1.48324	2.665
H	3.38563	1.35663	1.57526
H	2.62095	0.68149	3.02424
H	-0.59771	-0.50472	-0.4876

Atomic Coordinates of **SMa-deprot**:

C	-3.31154	-0.77628	-0.56042
C	-1.99125	-1.33099	-0.40231
C	-1.82734	-2.67053	0.0033
C	-2.95801	-3.44089	0.24672
C	-4.25814	-2.90063	0.09329
C	-4.4417	-1.58274	-0.30576
C	-3.1072	0.56981	-0.97139
C	-1.71869	0.74186	-1.03813
H	-0.82987	-3.08969	0.12199
H	-2.8457	-4.47659	0.55996
H	-5.12286	-3.53027	0.29128
H	-5.44625	-1.17862	-0.42065
H	-3.85716	1.31806	-1.19713
N	-1.02241	-0.40313	-0.69275
C	-1.03085	1.93476	-1.41036
C	-0.45505	2.95667	-1.73049
C	0.23688	4.18522	-2.11616
H	1.24062	4.2321	-1.67622
H	0.35146	4.26156	-3.20504
H	-0.3112	5.07427	-1.78054
C	-2.33647	2.2963	1.88789
O	-3.03038	3.13335	1.4593
O	-1.6415	1.47545	2.34722
C	2.25945	-0.46835	0.11202
N	1.36095	-0.05552	1.02225
H	0.38611	-0.05261	0.69483
N	1.79451	-0.85028	-1.08617
N	3.57531	-0.50042	0.39865
C	1.73331	0.46007	2.33386
C	4.08554	-0.12654	1.72672
C	3.00378	-0.24782	2.79734
C	4.56842	-0.9005	-0.61004
C	2.65352	-1.35647	-2.14943
C	4.0317	-0.7109	-2.02691
H	2.1864	-1.10939	-3.10635
H	2.73543	-2.45067	-2.09131
H	3.95651	0.35829	-2.25464
H	4.72819	-1.15976	-2.74084
H	5.45899	-0.2836	-0.45439
H	4.85528	-1.94642	-0.43744
H	4.92323	-0.79316	1.95509
H	4.47964	0.89758	1.68379
H	3.3676	0.19306	3.72986
H	2.78486	-1.30469	2.98623
H	1.89107	1.54676	2.29168
H	0.90192	0.27239	3.01717
H	0.76417	-0.77596	-1.19191

Atomic Coordinates of **TS1**:

C	-3.23896	-0.3926	-0.36799
C	-2.05514	-0.93043	-0.95051
C	-1.95872	-2.29479	-1.26096
C	-3.05981	-3.10874	-1.00625
C	-4.24017	-2.57935	-0.44499
C	-4.33693	-1.22813	-0.11685
C	-2.94253	1.00344	-0.11546
C	-1.66009	1.20719	-0.73742
H	-1.04901	-2.69983	-1.69747
H	-3.01199	-4.16788	-1.24683
H	-5.08661	-3.23766	-0.26558
H	-5.24912	-0.83225	0.3241
H	-3.67998	1.78724	-0.00168
N	-1.10062	0.05899	-1.15841
C	-0.9795	2.45401	-0.83217
C	-0.42575	3.53182	-0.91521
C	0.24597	4.82448	-1.01311
H	1.0262	4.80808	-1.78306
H	-0.4619	5.62124	-1.27084
H	0.72161	5.0982	-0.06329
C	-2.31031	0.95154	1.87812
O	-3.03968	1.71582	2.45432
O	-1.39479	0.17125	1.99162
C	2.21014	-0.4604	0.06447
N	1.36309	-0.31259	1.09987
H	0.37558	-0.16064	0.9091
N	1.71683	-0.40822	-1.1792
N	3.52577	-0.66049	0.28525
C	1.80385	-0.26627	2.49105
C	4.08266	-0.80005	1.64039
C	3.00992	-1.18454	2.65434
C	4.4891	-0.74791	-0.82344
C	2.54186	-0.59436	-2.36873
C	3.9514	-0.0836	-2.08674
H	2.07461	-0.03994	-3.18671
H	2.56818	-1.65431	-2.65661
H	3.92809	1.00399	-1.95556
H	4.61581	-0.30864	-2.92587
H	5.40951	-0.25488	-0.49475
H	4.72688	-1.80394	-1.00805
H	4.86006	-1.56965	1.5957
H	4.56718	0.14353	1.92449
H	3.42086	-1.10082	3.66445
H	2.70254	-2.22473	2.49921
H	2.06123	0.76248	2.77861
H	0.96377	-0.58558	3.11015
H	0.69486	-0.23227	-1.28078

Atomic Coordinates of **Int1a**:

C	-3.15142	-0.47431	-0.0675
C	-2.16601	-1.1144	-0.8452
C	-2.1685	-2.49582	-1.03448
C	-3.19038	-3.23489	-0.42973
C	-4.17356	-2.60414	0.34511
C	-4.15793	-1.21586	0.53953
C	-2.79161	0.98219	-0.02611
C	-1.63169	1.00249	-0.98681
H	-1.40335	-2.97726	-1.63671
H	-3.22287	-4.31274	-0.56307
H	-4.95794	-3.20018	0.80354
H	-4.91399	-0.73374	1.15326
H	-3.59494	1.67582	-0.28235
N	-1.24645	-0.18747	-1.38372
C	-0.95467	2.19055	-1.36258
C	-0.42162	3.23588	-1.67565
C	0.23524	4.48101	-2.05465
H	-0.3562	5.35067	-1.74731
H	1.22219	4.56056	-1.58332
H	0.37965	4.53424	-3.14007
C	-2.2953	1.34422	1.46596
O	-3.16358	1.84838	2.19499
O	-1.10513	1.03503	1.73679
C	2.19745	-0.37109	0.17127
N	1.45962	0.24226	1.10745
H	0.45039	0.39964	0.98602
N	1.62589	-0.7213	-0.99336
N	3.50468	-0.62938	0.39233
C	2.01614	0.70333	2.3776
C	4.14809	-0.36987	1.69073
C	3.12406	-0.24786	2.81352
C	4.37648	-1.20813	-0.64224
C	2.33634	-1.44821	-2.04187
C	3.79873	-1.0176	-2.04002
H	1.85141	-1.21224	-2.99225
H	2.25399	-2.53226	-1.88356
H	3.87186	0.03442	-2.33734
H	4.37514	-1.61206	-2.75454
H	5.35086	-0.71543	-0.55987
H	4.52608	-2.27412	-0.42489
H	4.83471	-1.20044	1.88504
H	4.75022	0.54491	1.61135
H	3.61827	0.12356	3.7158
H	2.69693	-1.23086	3.04142
H	2.40658	1.72526	2.27516
H	1.19084	0.73152	3.09083
H	0.63466	-0.50029	-1.15164

Atomic Coordinates of **Int1b**:

C	1.70899	-1.39662	-0.10319
C	2.94452	-1.43389	-0.77455
C	3.48473	-2.58867	-1.33485
C	2.72914	-3.75457	-1.21038
C	1.49112	-3.74604	-0.54606
C	0.97281	-2.57554	0.01369
C	1.47589	-0.00648	0.38195
C	2.64306	0.71797	-0.13513
H	4.44294	-2.58264	-1.84434
H	3.10593	-4.6809	-1.63326
H	0.92655	-4.67053	-0.46546
H	0.02511	-2.57704	0.53968
H	0.50354	0.44936	0.07052
N	3.46764	-0.13151	-0.75793
C	2.92549	2.08499	-0.01928
C	3.14878	3.27621	0.06605
C	3.42028	4.70017	0.17831
H	2.4884	5.27182	0.24762
H	4.01081	4.90522	1.07943
H	3.98746	5.06106	-0.68668
C	1.27597	0.07702	2.05345
O	0.34282	-0.65897	2.42274
O	2.03334	0.83889	2.65408
C	-2.44152	0.42008	0.02256
N	-2.34538	-0.21056	1.24397
H	-1.38932	-0.33806	1.57863
N	-1.36999	0.99649	-0.45407
N	-3.68544	0.43498	-0.5752
C	-3.3548	-1.14406	1.7146
H	-3.29193	-2.12303	1.20885
H	-3.18534	-1.3177	2.78178
C	-4.87239	-0.21926	-0.01892
H	-5.73496	0.43807	-0.19003
H	-5.0685	-1.15107	-0.57368
C	-4.7257	-0.52283	1.46886
H	-4.81124	0.39965	2.05455
H	-5.52764	-1.1993	1.78181
C	-3.8567	0.97911	-1.92437
H	-4.53041	0.31109	-2.47674
H	-4.35484	1.95902	-1.86702
C	-1.50169	1.74011	-1.69791
H	-0.51543	1.79101	-2.17721
H	-1.7994	2.78543	-1.50103
C	-2.51881	1.1026	-2.64694
H	-2.64617	1.69398	-3.56061
H	-2.1635	0.10665	-2.93993
H	4.35583	0.14097	-1.16631

Atomic Coordinates of **TS2**:

C	-1.45039	1.53883	0.06467
C	-2.50688	1.63169	-0.86191
C	-2.83251	2.80028	-1.54819
C	-2.05058	3.92209	-1.27774
C	-0.99276	3.86021	-0.35343
C	-0.68279	2.67766	0.3207
C	-1.38904	0.14009	0.56818
C	-2.51656	-0.50143	-0.1014
H	-3.65482	2.83524	-2.25599
H	-2.26553	4.85691	-1.78678
H	-0.40573	4.75363	-0.15987
H	0.12335	2.63369	1.04336
H	-0.38157	-0.38826	0.19139
N	-3.11658	0.37383	-0.92548
C	-2.95142	-1.83223	-0.00184
C	-3.33194	-2.98439	0.05353
C	-3.78121	-4.36583	0.13255
H	-3.54995	-4.79683	1.1129
H	-4.86222	-4.43661	-0.03122
H	-3.28425	-4.97619	-0.63107
C	-1.16636	-0.0949	2.14192
O	-0.22904	0.60048	2.61006
O	-1.89931	-0.92539	2.69542
C	2.19975	-0.52029	0.03637
N	2.2736	0.18683	1.20196
H	1.38616	0.33986	1.69233
N	1.03998	-1.0452	-0.29776
N	3.3515	-0.66715	-0.69644
C	3.4402	0.96202	1.58667
H	3.46123	1.9472	1.09242
H	3.38814	1.13958	2.66501
C	4.65684	-0.15208	-0.27175
H	5.414	-0.90785	-0.51601
H	4.90064	0.74681	-0.85884
C	4.6911	0.16971	1.21907
H	4.71636	-0.75636	1.80476
H	5.59754	0.73954	1.44668
C	3.32579	-1.2921	-2.02182
H	3.9929	-0.7183	-2.67728
H	3.73678	-2.31071	-1.95606
C	0.95716	-1.83801	-1.51385
H	-0.07983	-1.80699	-1.87264
H	1.17895	-2.8983	-1.30489
C	1.91176	-1.32259	-2.59216
H	1.88895	-1.95635	-3.48536
H	1.60982	-0.31104	-2.89024
H	-3.90443	0.1401	-1.51969

Atomic Coordinates of **Int2**:

C	-1.43844	1.44162	0.62809
C	-2.22633	1.94234	-0.44719
C	-2.10921	3.25436	-0.92253
C	-1.1826	4.08036	-0.29644
C	-0.39402	3.61087	0.77743
C	-0.51122	2.30717	1.24281
C	-1.82884	0.06804	0.85068
C	-2.83128	-0.20778	-0.0823
H	-2.72179	3.61145	-1.74559
H	-1.06545	5.10519	-0.63825
H	0.31762	4.28571	1.2461
H	0.09034	1.94036	2.06645
H	0.27745	-0.33438	-0.34418
N	-3.05307	0.92209	-0.8571
C	-3.57939	-1.38244	-0.33711
C	-4.26197	-2.34312	-0.62946
C	-5.06974	-3.51504	-0.95192
H	-4.99034	-4.27549	-0.16627
H	-6.12887	-3.25037	-1.05544
H	-4.74863	-3.97403	-1.89494
C	-1.30174	-0.86895	1.90917
O	-0.17935	-0.54146	2.43588
O	-1.98047	-1.87611	2.20229
C	2.28964	-0.47853	-0.16323
N	2.22192	-0.37041	1.16693
H	1.2776	-0.39039	1.61552
N	1.13773	-0.47103	-0.86392
N	3.47095	-0.58656	-0.80211
C	3.40793	-0.3634	2.0186
H	3.751	0.66645	2.18634
H	3.11894	-0.77915	2.98708
C	4.73776	-0.70235	-0.06214
H	5.37255	-1.40484	-0.61147
H	5.24269	0.27257	-0.06432
C	4.50845	-1.19331	1.36404
H	4.21437	-2.2488	1.35196
H	5.44036	-1.10899	1.93027
C	3.56662	-0.61818	-2.26991
H	4.46374	-0.05708	-2.55025
H	3.71014	-1.65688	-2.59582
C	1.07388	-0.61868	-2.31571
H	0.17512	-0.10427	-2.66325
H	0.98389	-1.67814	-2.59003
C	2.33181	-0.00939	-2.92672
H	2.36278	-0.20075	-4.00299
H	2.32405	1.0756	-2.77514
H	-3.71963	0.96655	-1.61484

Atomic Coordinates of **TS3**:

C	3.47552	-0.66009	0.07434
C	4.71148	0.04973	0.02427
C	5.94837	-0.59714	0.09358
C	5.94451	-1.98557	0.21582
C	4.73537	-2.70759	0.26741
C	3.5045	-2.05984	0.19825
C	2.43521	0.33187	-0.02156
C	3.04994	1.58499	-0.12662
H	6.87906	-0.03749	0.05363
H	6.89003	-2.5183	0.27221
H	4.76683	-3.79001	0.3631
H	2.57289	-2.61444	0.23823
H	-1.23679	-1.17459	-0.21969
N	4.41441	1.3964	-0.09761
C	2.39912	2.85317	-0.25056
C	1.10995	2.87233	-0.25925
C	-0.06252	3.76731	-0.34573
H	-0.7273	3.49223	-1.17303
H	-0.65617	3.75471	0.57705
H	0.28577	4.79178	-0.50971
C	0.99168	0.17167	-0.02343
O	0.46618	-0.96827	0.05605
O	0.25394	1.25707	-0.11165
C	-3.10777	-0.3916	0.00207
N	-2.60873	0.8204	0.30205
H	-1.59866	0.96515	0.18001
N	-2.25137	-1.36299	-0.3397
N	-4.43713	-0.61771	0.04151
C	-3.44713	1.92937	0.74726
H	-3.56629	1.90861	1.83918
H	-2.93679	2.85887	0.48626
C	-5.40725	0.45551	0.30762
H	-6.26808	0.28949	-0.34845
H	-5.75941	0.36637	1.34396
C	-4.80527	1.83436	0.05827
H	-4.68145	2.00131	-1.0175
H	-5.48463	2.60036	0.44297
C	-5.00234	-1.95955	-0.17185
H	-5.83865	-2.07635	0.52517
H	-5.41014	-2.01596	-1.18988
C	-2.68798	-2.70539	-0.71025
H	-1.87677	-3.39582	-0.46662
H	-2.86315	-2.76589	-1.79306
C	-3.96153	-3.05139	0.05576
H	-4.36455	-4.01104	-0.28044
H	-3.73481	-3.13524	1.1245
H	5.08485	2.15011	-0.15918

Atomic Coordinates of **Int3a**:

C	3.55908	-0.67306	0.15799
C	4.73409	0.11298	-0.09654
C	6.00042	-0.49379	-0.06084
C	6.08802	-1.85566	0.22272
C	4.93242	-2.62427	0.47216
C	3.66577	-2.04175	0.44177
C	2.47939	0.2667	0.03858
C	3.1057	1.51698	-0.27507
H	6.89354	0.09671	-0.253
H	7.06363	-2.33563	0.25289
H	5.03252	-3.68489	0.69063
H	2.77478	-2.63423	0.63373
H	-1.26891	-1.17754	-0.13237
N	4.44093	1.44522	-0.35991
C	2.27573	2.67297	-0.46748
C	0.93554	2.54177	-0.33939
C	-0.08347	3.62406	-0.49771
H	-0.82318	3.35874	-1.26301
H	-0.62706	3.79502	0.44045
H	0.39895	4.56006	-0.78932
C	1.09046	0.13971	0.16279
O	0.40645	-0.86395	0.424
O	0.35149	1.32887	-0.03123
C	-3.13624	-0.41125	0.05616
N	-2.65147	0.74866	0.53744
H	-1.64692	0.89369	0.48225
N	-2.26315	-1.34642	-0.34164
N	-4.46356	-0.61763	-0.02342
C	-3.50678	1.81773	1.04758
H	-3.70184	1.67303	2.11827
H	-2.96904	2.76094	0.92985
C	-5.44112	0.43376	0.30237
H	-6.25547	0.35892	-0.4254
H	-5.8635	0.22786	1.29451
C	-4.81229	1.82275	0.25805
H	-4.61084	2.1109	-0.77958
H	-5.51165	2.54922	0.68119
C	-5.02122	-1.91596	-0.43737
H	-5.90601	-2.10212	0.17982
H	-5.35412	-1.84133	-1.48074
C	-2.67798	-2.6324	-0.89699
H	-1.89201	-3.35779	-0.67469
H	-2.77099	-2.56344	-1.98889
C	-4.00687	-3.04299	-0.26935
H	-4.39178	-3.94918	-0.74553
H	-3.85863	-3.25673	0.79496
H	2.70183	3.63988	-0.71222

Atomic Coordinates of **Int3b**:

C	-2.80095	-1.30307	-0.10971
C	-1.39343	-1.57064	-0.13834
C	-0.92717	-2.88876	-0.25634
C	-1.85832	-3.92226	-0.3454
C	-3.24344	-3.66004	-0.3188
C	-3.72274	-2.35648	-0.20142
C	-2.89318	0.12463	0.01897
C	-1.55459	0.5939	0.05622
H	0.14068	-3.09479	-0.27718
H	-1.51156	-4.94892	-0.43704
H	-3.94526	-4.48753	-0.39057
H	-4.78988	-2.15247	-0.18068
H	1.0374	-0.07912	-1.05217
N	-0.64247	-0.40299	-0.03651
C	-1.30405	1.99997	0.17959
C	-2.37066	2.83268	0.25717
C	-2.31773	4.32228	0.38745
H	-2.83337	4.80557	-0.45154
H	-2.81702	4.65151	1.30709
H	-1.28191	4.66974	0.40817
C	-4.00217	1.00144	0.10259
O	-5.20329	0.75245	0.08691
O	-3.66044	2.37293	0.22245
C	2.7496	-0.01405	-0.0095
N	2.06586	-0.2735	1.11669
H	1.04718	-0.36009	0.99293
N	2.0496	0.07839	-1.15202
N	4.08536	0.14823	0.00601
C	2.69167	-0.34672	2.43202
H	2.68684	0.63913	2.91676
H	2.09804	-1.02498	3.05012
C	4.86404	-0.00432	1.24524
H	5.81515	-0.4744	0.97658
H	5.0885	0.99046	1.65215
C	4.12117	-0.85743	2.27043
H	4.10114	-1.90163	1.93921
H	4.65031	-0.81653	3.22664
C	4.83461	0.48131	-1.21584
H	5.63771	1.16746	-0.92926
H	5.30251	-0.43082	-1.60918
C	2.67156	0.29107	-2.45373
H	1.94891	0.80517	-3.09235
H	2.91298	-0.67022	-2.92761
C	3.93423	1.12803	-2.2656
H	4.48077	1.20977	-3.20935
H	3.65831	2.13919	-1.94622
H	-0.29676	2.40033	0.20946

Supplementary Information References:

1. Fang, Y., Lautens, M. *J. Org. Chem.* **2008,** 73, 2, 538-549.
2. Grover, H. K., Lebold, T. P., Kerr, M. A. *Org. Lett.* **2011,** 13, 2, 220-23.
3. Villiers, C., Dognon, J., Pollet, R., Thuery, P., Ephritikhine, M. *Angew. Chem. Int. Ed.* **2010,** 49, 3465-3468.
4. Sadamitsu, K., Komatsuki, K., Saito, K., Yamada, T. *Org. Lett.* **2017,** 19, 3191-3194.
5. Only the trans isomer was fully characterized due to the rapid isomerization of the alkene under reaction conditions.
6. Furche, F. *WIREs Comput. Mol. Sci.* **2013,** 4, 2, 91-100.
7. Perdew, J. P. *Phys. Rev. B.* **1986,** 33, 8822-8824.
8. Becke, A. D. *Phys. Rev. A.* **1988,** 38, 6, 3098-3100.
9. Rappoport, D., Furche, F. *J. Chem. Phys.* **2010,** 133, 13, 3405-3410.
10. Weigend, F., Ahlrichs, R. *Phys. Chem. Chem. Phys.* **2005,** 7, 18, 3297-3305.